

The Remarkably Strong Arctic Stratospheric Polar Vortex of Winter 2020: Links to Record-Breaking Arctic Oscillation and Ozone Loss

Zachary Duane Lawrence¹, Judith Perlwitz², Amy Hawes Butler¹, Gloria L Manney³, Paul A. Newman⁴, Simon Haydn Lee⁵, and Eric R Nash⁶

¹CIRES/NOAA

²National Oceanic and Atmospheric Administration (NOAA)

³Northwest Research Associates

⁴National Aeronautics and Space Administration (NASA)

⁵University of Reading

⁶SSAI

November 24, 2022

Abstract

The Northern Hemisphere (NH) polar winter stratosphere of 2019/2020 featured an exceptionally strong and cold stratospheric polar vortex. Wave activity from the troposphere during December–February was unusually low, which allowed the polar vortex to remain relatively undisturbed. Several transient wave pulses nonetheless served to help create a reflective configuration of the stratospheric circulation by disturbing the vortex in the upper stratosphere. Subsequently, multiple downward wave coupling events took place, which aided in dynamically cooling and strengthening the polar vortex. The persistent strength of the stratospheric polar vortex was accompanied by an unprecedentedly positive phase of the Arctic Oscillation in the troposphere during January–March, which was consistent with large portions of observed surface temperature and precipitation anomalies during the season. Similarly, conditions within the strong polar vortex were ripe for allowing substantial ozone loss: The undisturbed vortex was a strong transport barrier, and temperatures were low enough to form polar stratospheric clouds for over four months into late March. Total column ozone amounts in the NH polar cap decreased, and were the lowest ever observed in the February–April period. The unique confluence of conditions and multiple broken records makes the 2019/2020 winter and early spring a particularly extreme example of two-way coupling between the troposphere and stratosphere.

1 **The Remarkably Strong Arctic Stratospheric Polar**
2 **Vortex of Winter 2020: Links to Record-Breaking**
3 **Arctic Oscillation and Ozone Loss**

4 **Zachary D. Lawrence^{1,2}, Judith Perlwitz², Amy H. Butler³, Gloria L.**
5 **Manney^{4,5}, Paul A. Newman⁶, Simon H. Lee⁷, Eric R. Nash^{6,8}**

6 ¹Cooperative Institute for Research in Environmental Sciences (CIRES), University of Colorado, Boulder,
7 Colorado, USA

8 ²NOAA Physical Sciences Laboratory (PSL), Boulder, Colorado, USA

9 ³NOAA Chemical Sciences Laboratory (CSL), Boulder, Colorado, USA

10 ⁴NorthWest Research Associates (NWRA), Socorro, New Mexico, USA

11 ⁵New Mexico Tech (NMT), Socorro, New Mexico, USA

12 ⁶NASA, Goddard Space Flight Center (GSFC), Greenbelt, Maryland, USA

13 ⁷Department of Meteorology, University of Reading, Reading, UK

14 ⁸Science Systems and Applications, Inc. (SSAI), Lanham, Maryland, USA

15 **Key Points:**

- 16 • The Arctic stratospheric polar vortex during the 2019/2020 winter was the strongest
17 and most persistently cold in over 40 years
- 18 • Low tropospheric planetary wave driving and a wave-reflecting configuration of
19 the polar stratosphere contributed to the strong and cold polar vortex
- 20 • Seasonal records in the Arctic Oscillation and stratospheric ozone loss were related
21 to the strong polar vortex

Corresponding author: Zachary Lawrence, zachary.lawrence@noaa.gov

Abstract

The Northern Hemisphere (NH) polar winter stratosphere of 2019/2020 featured an exceptionally strong and cold stratospheric polar vortex. Wave activity from the troposphere during December-February was unusually low, which allowed the polar vortex to remain relatively undisturbed. Several transient wave pulses nonetheless served to help create a reflective configuration of the stratospheric circulation by disturbing the vortex in the upper stratosphere. Subsequently, multiple downward wave coupling events took place, which aided in dynamically cooling and strengthening the polar vortex. The persistent strength of the stratospheric polar vortex was accompanied by an unprecedentedly positive phase of the Arctic Oscillation in the troposphere during January-March, which was consistent with large portions of observed surface temperature and precipitation anomalies during the season. Similarly, conditions within the strong polar vortex were ripe for allowing substantial ozone loss: The undisturbed vortex was a strong transport barrier, and temperatures were low enough to form polar stratospheric clouds for over four months into late March. Total column ozone amounts in the NH polar cap decreased, and were the lowest ever observed in the February-April period. The unique confluence of conditions and multiple broken records makes the 2019/2020 winter and early spring a particularly extreme example of two-way coupling between the troposphere and stratosphere.

Plain Language Summary

Wintertime westerly winds in the polar stratosphere (from roughly 15-50km), known as the stratospheric polar vortex, were extraordinarily strong during the Northern Hemisphere (NH) winter of 2019/2020. The exceptional strength of the stratospheric polar vortex had consequences for winter and early spring weather near the surface, and for stratospheric ozone depletion. Typically atmospheric waves generated in the troposphere spread outward and upward into the stratosphere where they can disturb and weaken the polar vortex, but wave activity from the troposphere was unusually weak during the 2019/2020 winter. In addition, an unusual configuration of the stratospheric polar vortex developed that was able to reflect waves traveling upward from the troposphere back downward. These unique conditions allowed the vortex to remain strong and cold for several months. During January-March 2020, the strong stratospheric polar vortex was closely linked to a near surface circulation pattern that resembles the positive phase of the so-called “Arctic Oscillation” (AO). This positive AO pattern was also of record strength, and influenced the regional distributions of temperatures and precipitation during the late winter and early spring. Cold and stable conditions within the polar vortex also allowed strong ozone depletion to take place, leading to lower ozone levels than ever before seen above the Arctic in spring.

1 Introduction

The Northern Hemisphere (NH) late winter and spring of 2020 featured a series of remarkable climate extremes. The tropospheric Arctic Oscillation – the dominant pattern of extratropical climate variability that describes the latitudinal shift of the eddy-driven jet stream (AO; Thompson & Wallace, 1998) – was effectively locked in a highly positive phase for several months. Stratospheric ozone in the polar cap fell to low levels never before observed in early NH spring. These phenomena were connected by the Arctic stratospheric polar vortex, which was unusually and persistently strong and cold during the season. This paper provides an overview of the 2019/2020 record breaking strong stratospheric polar vortex event and its connections to the extremes in the tropospheric AO and Arctic ozone.

During winter, the stratospheric and tropospheric circulation are closely connected. The stratospheric polar vortex (hereinafter, simply the polar vortex) is the principal feature of the polar wintertime stratosphere, consisting of a strong westerly circulation span-

72 ning from roughly 100 hPa to above 1 hPa (Vaugh et al., 2017). Polar vortex strength
 73 is primarily modulated by dynamical troposphere-stratosphere coupling via planetary
 74 scale waves generated in the troposphere from orography and sources of diabatic heat-
 75 ing (e.g., Charney & Drazin, 1961; Matsuno, 1970). Waves from the troposphere can prop-
 76 agate vertically into the polar stratosphere, where they can break and disturb the po-
 77 lar vortex. The polar vortex strengthens and cools during polar night via radiative cool-
 78 ing, but breaking waves deposit easterly momentum, weakening the westerly zonal cir-
 79 culation represented by the polar vortex, and warming the polar stratosphere. As a re-
 80 sult, reduced wave driving allows the polar vortex to more closely approach the very cold
 81 conditions of radiative equilibrium. Processes internal to the stratosphere that involve
 82 the interplay between dynamic driving and radiative relaxation can also play a role, as
 83 wave propagation characteristics are modulated by the basic state flow. For example,
 84 downward wave coupling events in which waves are reflected downward from the strato-
 85 sphere can strengthen the vortex (Shaw & Perlwitz, 2014; Dunn-Sigouin & Shaw, 2015);
 86 these events have been shown to be preceded by transient pulses of upward wave activ-
 87 ity that help develop reflective configurations of the polar stratospheric circulation (Harnik,
 88 2009; Shaw et al., 2010; Shaw & Perlwitz, 2013).

89 A main expression of two-way stratosphere-troposphere dynamical coupling dur-
 90 ing NH winter is the close statistical relationship between the strength of the stratospheric
 91 polar vortex and the phase of the AO (e.g., Baldwin & Dunkerton, 2001; Kidston et al.,
 92 2015). Anomalously strong or weak stratospheric polar vortex states tend to be followed
 93 in the troposphere by positive or negative AO events that can last for weeks to months
 94 and alter patterns of surface temperatures and precipitation. These relationships are gen-
 95 erally expressed using metrics that describe phases of the “Northern Annular Mode” (NAM),
 96 a pattern that characterizes meridional shifts of mass into or out of the polar cap through-
 97 out the atmospheric column (note that the NAM and AO are often used interchange-
 98 ably; Thompson & Wallace, 2000; Baldwin, 2001). As a result, the strength of the NH
 99 polar vortex is generally recognized as an important element for coupling between the
 100 stratosphere and troposphere on sub-seasonal to seasonal timescales during winter and
 101 spring (e.g., Kidston et al., 2015; Butler et al., 2019).

102 Extreme mid-winter weak vortex events, called sudden stratospheric warmings (SSWs),
 103 lead to a negative-NAM stratospheric state that can help drive a persistent negative AO/NAM
 104 in the troposphere, and increase the probability of events such as mid-latitude cold air
 105 outbreaks (e.g., Kidston et al., 2015; Domeisen, 2019; King et al., 2019). SSWs are quite
 106 common in the NH, occurring in roughly 6 out of every 10 years (Butler et al., 2017).
 107 Anomalously strong states of the polar vortex (positive phases of the stratospheric NAM)
 108 have similarly been shown to help influence or induce positive AO/NAM states in the
 109 troposphere (Baldwin & Dunkerton, 2001; Polvani & Kushner, 2002; Limpasuvan et al.,
 110 2005; Dunn-Sigouin & Shaw, 2015; Tripathi, Charlton-Perez, et al., 2015; Orsolini et al.,
 111 2018). However, *persistent* strong events like that observed during the winter and spring
 112 of 2020 are quite rare in comparison to SSWs: since SSWs often lead to a nearly com-
 113 plete breakdown of the polar vortex, the timescale of recovery from a weak stratospheric
 114 circulation can be quite long (Hitchcock & Shepherd, 2013; Hitchcock et al., 2013). In
 115 contrast, the polar vortex can shift from a strong state to a neutral or weak state on very
 116 short timescales (Limpasuvan et al., 2005; Lawrence & Manney, 2018). Factors that seem
 117 to determine whether a given vortex event will influence the troposphere include the per-
 118 sistence and magnitude of stratospheric anomalies, the depth to which anomalies pen-
 119 etrate into the lower stratosphere, and the tropospheric state at the time of the event
 120 (e.g., Karpechko et al., 2017; Charlton-Perez et al., 2018; Domeisen, 2019; White et al.,
 121 2019; Rao et al., 2020), although these factors have generally been determined from the
 122 study of SSW events.

123 The conditions that determine the potential for chemical ozone destruction in the
 124 NH stratosphere also tie in to polar vortex strength, albeit in subtle ways that are highly

125 sensitive to meteorology (WMO, 2014, 2018). Chlorine and bromine trace gases, primar-
 126 ily from anthropogenic sources, are converted from reservoir (non-ozone depleting) forms
 127 to reactive (ozone-depleting) forms on the surfaces of polar stratospheric clouds (PSCs;
 128 e.g., Solomon, 1999), which require very low temperatures (~ 195 K) to form in the lower
 129 stratosphere. Activation of chlorine/bromine also generally requires persistent confine-
 130 ment with cold air inside the polar vortex so that mixing with low latitude air cannot
 131 dilute the “activated air” (Schoeberl & Hartmann, 1991; Schoeberl et al., 1992). The chem-
 132 ical reactions that destroy ozone further require sunlight exposure, such that chemical
 133 ozone loss tends to dominate when sunlight returns to the polar regions in early spring,
 134 a time when, climatologically, the Arctic vortex is often very weak or broken down al-
 135 together (Black et al., 2006; Lawrence et al., 2018). The aforementioned conditions for
 136 ozone destruction are typically only present when the polar vortex is strong, cold, and
 137 stable, but the interannual variability in the Arctic polar vortex is so large that individ-
 138 ual seasons can have individual conditions present without the others: For example, the
 139 polar vortex in 2015/2016 was persistently strong and cold for much of the season, but
 140 a dynamically driven early final warming occurred in the beginning of March, which cut
 141 short the chemical ozone loss, broke down the vortex, and dispersed the air previously
 142 within it (Manney & Lawrence, 2016), preventing an extreme ozone deficit.

143 In this paper we will show that the 2019/2020 record breaking strong vortex de-
 144 veloped in the wake of a combination of low wave driving from the troposphere and the
 145 formation of a reflective configuration in the upper stratospheric circulation. The record-
 146 breaking strength of the vortex was accompanied by a record-breaking positive phase
 147 of the tropospheric AO that lasted several months and was related to large fractions of
 148 NH seasonal surface temperatures and precipitation anomalies. We will further illustrate
 149 that the strong and stable vortex also provided conditions that were ideal for chemical
 150 ozone loss to take place, resulting in the lowest Arctic ozone amounts on record during
 151 late winter and early spring. That the record-breaking AO and low ozone events took
 152 place individually is notable, but that they both occurred during the same season makes
 153 the 2019/2020 Arctic winter particularly extraordinary.

154 The rest of the paper is organized as follows: Section 2 outlines the datasets and
 155 methods we use. Section 3 is broken into subsections that focus on describing the record
 156 strength of the vortex (Section 3.1); the coupled troposphere-stratosphere evolution (Sec-
 157 tion 3.2); the influence of two-way wave coupling on the vortex (Section 3.3); and the
 158 vortex conditions that were conducive for ozone loss (Section 3.4). Finally, in Section 4
 159 we summarize our results and provide some research questions that are motivated by this
 160 record-breaking winter and early spring.

161 2 Data and Methods

162 We combine data from multiple sources to analyze the conditions during the 2019/2020
 163 Arctic winter, and to provide historical context from previous winters. Meteorological
 164 variables such as temperatures, winds, and geopotential height are from the National Aero-
 165 nautics and Space Administration (NASA) Modern-Era Retrospective analysis for Re-
 166 search and Applications version 2 (MERRA-2; Gelaro et al., 2017). We specifically use
 167 daily mean fields from the pressure (“M2I3NPASM”; GMAO, 2020b) and model (“M2I3NVASM”
 168 GMAO, 2020a) level collections. For historical context of stratospheric zonal mean zonal
 169 winds from previous winters, we also utilize daily mean pressure level data from the Japanese
 170 Meteorological Agency’s 55-year reanalysis (JRA-55; Kobayashi et al., 2015) for win-
 171 ter seasons from 1958/1959 to 1978/1979. Ozone data and statistics are compiled from
 172 multiple satellite instruments, but are primarily from the Ozone Mapping and Profiling
 173 Suite (OMPS) from data made available via the NASA OzoneWatch resource (see, e.g.,
 174 <https://ozonewatch.gsfc.nasa.gov/data/> and <https://ozonewatch.gsfc.nasa.gov/meteorology/figures/ozone/>); missing column ozone values in polar night are filled
 175 using MERRA-2 data. Daily values for the Arctic Oscillation index are provided by the
 176

177 National Centers for Environmental Prediction (NCEP) Climate Prediction Center (CPC)
 178 at https://www.cpc.ncep.noaa.gov/products/precip/CWlink/daily_ao_index/ao
 179 [.shtml](https://www.cpc.ncep.noaa.gov/products/precip/CWlink/daily_ao_index/ao.shtml).

180 We use diagnostics based on the Transformed Eulerian Mean (TEM) framework
 181 (Andrews et al., 1987), including Eliassen-Palm fluxes and residual velocities to describe
 182 the wave driving conditions and evolution of the stratospheric circulation during the 2019/2020
 183 winter season. We calculate these diagnostics based on the primitive equation formula-
 184 tion (see, e.g., Martineau et al., 2018) using MERRA-2 pressure level fields. We also use
 185 diagnostics of polar processing, which describe the development and maintenance of con-
 186 ditions that support chemical ozone loss; we compute these as described in Lawrence et
 187 al. (2018) using daily mean MERRA-2 data. Unless otherwise noted, we calculate anoma-
 188 lies with respect to climatologies using the full records available, but excluding 2020. Sim-
 189 ilarly, we use cosine-latitude weighted averages to calculate quantities representative of
 190 a range of latitudes. Note that the NAM and AO refer to identical phenomena (Baldwin,
 191 2001; Baldwin & Dunkerton, 2001), but herein we use the NAM to refer to the vertically
 192 resolved profile of mass fluctuations in the NH extratropical circulation, and the AO to
 193 refer to the near-surface pattern. We calculate the vertically resolved NAM index using
 194 standardized 65-90°N geopotential height anomalies as motivated by Cohen et al. (2002)
 195 and Baldwin and Thompson (2009), multiplied by -1 for consistent phasing with the AO.

196 3 Results

197 3.1 Strength of the 2019/2020 Polar Vortex in Context

198 In the middle stratosphere, zonal mean zonal winds were above average between
 199 60-65°N for the majority of the extended winter season, but became particularly strong
 200 around mid-January (Figure 1a). Beginning in January, polar vortex winds were regu-
 201 larly more than 20 m/s higher than those in the climatology. In February, the wind anoma-
 202 lies exceeded two standard deviations of the November-April climatology for over a full
 203 month and reached record maxima during a period of time in the seasonal cycle when
 204 winds in this altitude and latitude region generally decrease.

205 The temporal evolution of zonal wind anomalies at 60°N as a function of pressure
 206 reveals that the vortex was generally stronger than normal in the stratosphere between
 207 100 and 1 hPa from November to April (Fig 1b). The only exception is a short-lived vor-
 208 tex disturbance from mid-November to early December, as evidenced by negative wind
 209 anomalies between about 30 and 1 hPa at this time. Winds in the troposphere became
 210 anomalously positive for a brief period in early December, while more consistent pos-
 211 itive anomalies that often reached more than 10 m/s above normal became established
 212 in January.

213 Also notable is the zonal wind evolution in the upper stratosphere and lower meso-
 214 sphere (USLM; approximately pressures lower than 1 hPa). Following the short lived strato-
 215 spheric vortex disturbance in mid-November, winds in the USLM accelerated and briefly
 216 became very strong, reaching record high values and exceeding 2 standard deviations for
 217 a short time in mid-December. However, beginning in January, there is a clear contrast
 218 between winds in the USLM and the stratosphere; those in the USLM were generally weaker
 219 than normal, while those in the stratosphere proper were generally stronger than nor-
 220 mal, and reached record strength for periods in February and March.

221 The stratospheric circulation was clearly stronger than normal for almost the en-
 222 tirety of the extended December-March (DJFM) winter season. A comparison of zonal
 223 mean zonal winds across other winter seasons reveals that the polar vortex in 2020 was
 224 the strongest on record at 10 and 100 hPa for seasons back to 1979/1980 (Figure 2). This
 225 era is typically considered to be the “satellite-era”; when also including prior years back
 226 to 1958/1959 for which reanalysis data are more uncertain because of the relative lack

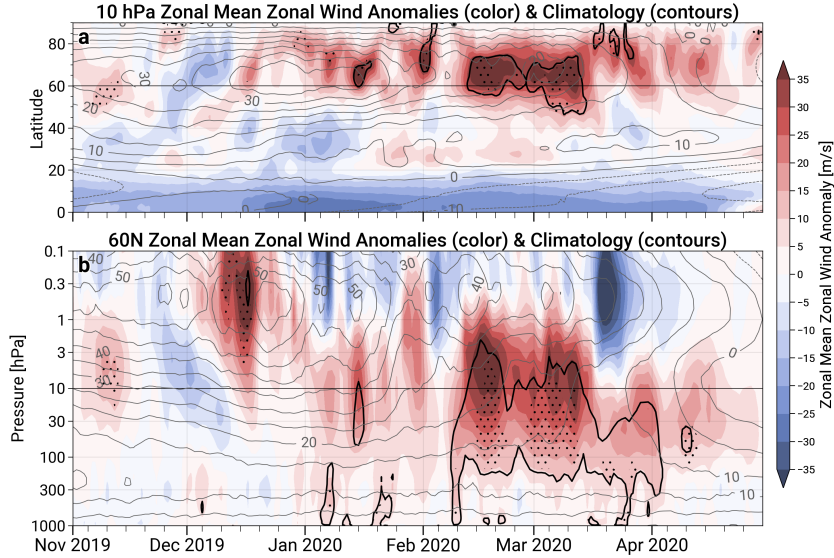


Figure 1. Time series of zonal mean zonal wind anomalies as a function of latitude at 10 hPa (a), and at 60°N as a function of pressure (b). The grey line contours represent the climatology; the black lines enclose the times when anomalies exceed +2 standard deviations of the November–April daily climatology; and stippling indicates when the zonal wind values were maxima in the MERRA-2 record.

227 of observations to constrain the reanalysis (see discussion in Hitchcock, 2019), the 2020
 228 zonal winds at 10 hPa rank third across all available years, only exceeded by 1966/1967
 229 and 1975/1976. At 100 hPa, the 2019/2020 zonal winds are the largest on record even
 230 when taking into account these earlier years. We note that in the post-1980 era, the dif-
 231 ferences in the seasonal zonal winds between MERRA-2 and JRA-55 are very small; the
 232 absolute maximum differences in the DJFM means are 0.6 m/s and 1.0 m/s at 10 and
 233 100 hPa, respectively, indicating that these results are robust between these two reanal-
 234 ysis data sets.

235 **3.2 An Extreme Event of the Coupled Troposphere-Stratosphere An-**
 236 **ular Mode**

237 The 2020 strong vortex event that developed in January and lasted through March
 238 was vertically coherent throughout the depth of the stratosphere. Moreover, the posi-
 239 tive zonal wind anomalies in the troposphere during this time indicate that the zonal pat-
 240 tern also extended into the troposphere (Figure 1). Figure 3a and b shows the coherent
 241 evolution of stratospheric and tropospheric circulation anomalies illustrated using indices
 242 of the NAM and AO, which clearly show a positive NAM/AO state between 1000 and
 243 1 hPa for almost the entire three months of JFM.

244 We use two diagnostics to illustrate how unusual this winter was with respect to
 245 the coupled stratosphere-troposphere NAM behaviour. First, we assess the influence of
 246 wave driving on the stratospheric polar vortex. Newman et al. (2001) showed that early
 247 spring polar stratospheric temperatures are highly correlated with time integrated eddy
 248 heat fluxes, revealing that interannual variability in spring polar stratospheric temper-
 249 atures is tied to the integrated amount of wave driving supplied by the troposphere and
 250 entering the stratosphere. Similarly, Polvani and Waugh (2004) showed a robust anti-

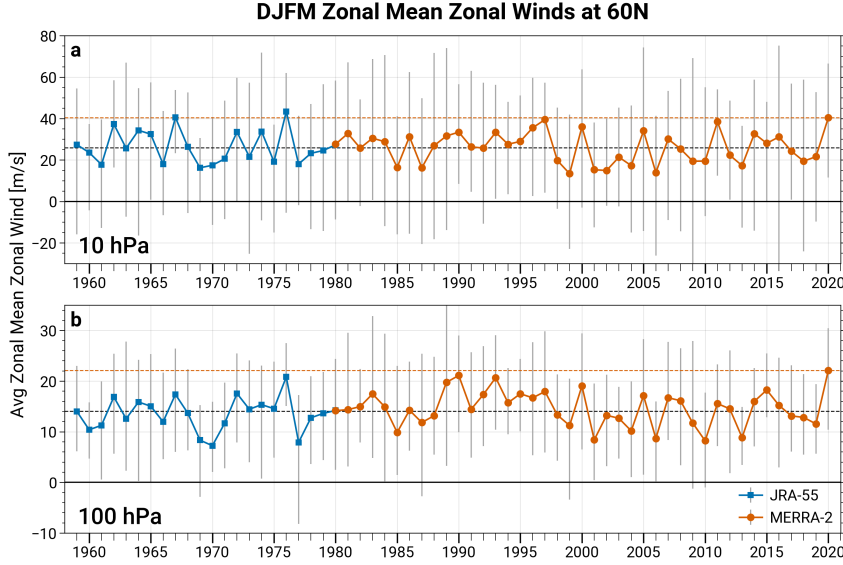


Figure 2. Yearly time series of the December-March averaged zonal mean zonal winds at $60^{\circ}N$, at 10 (a) and 100 (b) hPa. The blue lines and squares represent values determined from the JRA-55 reanalysis for 1959 through 1979; the orange lines and circles represent the values determined from MERRA-2. The grey whiskers in each panel represent the range of the daily mean zonal wind values during each season.

251 correlation between time integrated eddy heat fluxes and the stratospheric NAM, fur-
 252 ther indicating a control on the vortex strength by wave driving. Figure 3c supplements
 253 these relationships by displaying a scatterplot of the 100 hPa $40\text{-}80^{\circ}N$ vertical compo-
 254 nent of the Eliassen-Palm (EP) flux (F_z ; a diagnostic of vertical wave propagation) aver-
 255 aged over DJF versus the 50 hPa NAM averaged over JFM, which confirms a very close
 256 relationship ($r = -0.8$). Moreover, Figure 3c clearly illustrates that the 2020 winter sea-
 257 son represents a new extreme, with both the lowest DJF upward wave activity at 100
 258 hPa and the strongest 50 hPa NAM event in the MERRA-2 record.

259 Second, we put the 2020 coherent stratospheric and tropospheric NAM/AO behav-
 260 ior into context with previous years. Prior studies have shown that there is a significant
 261 statistical relationship between the strength of the stratospheric polar vortex (stratospheric
 262 NAM) and the AO on seasonal timescales (e.g., Thompson & Wallace, 1998). Figure 3d
 263 demonstrates this relationship as a scatterplot of JFM values of the 50 hPa NAM ver-
 264 sus polar cap sea level pressure (SLP). The correlation is approximately 0.68, and is sta-
 265 tistically significant at the 99% level following a bootstrap test of 50000 resamples. The
 266 JFM season of 2020 particularly stands out as the most extreme year in the MERRA-
 267 2 record, involving extremes in both the stratospheric NAM and negative sea level pres-
 268 sure anomalies. While this result does not imply a clear direction of influence or causal-
 269 ity, it is obvious from Figure 3a that the stratospheric anomalies were persistent, of large
 270 magnitude, and reached into the lower stratosphere. Similarly, a positive AO developed
 271 slightly before or simultaneous with the stratospheric anomalies in late December and
 272 early January, meaning that the tropospheric anomalies either developed in concert with
 273 the stratosphere, or was in a favorable state for coupling with a positive stratospheric
 274 NAM.

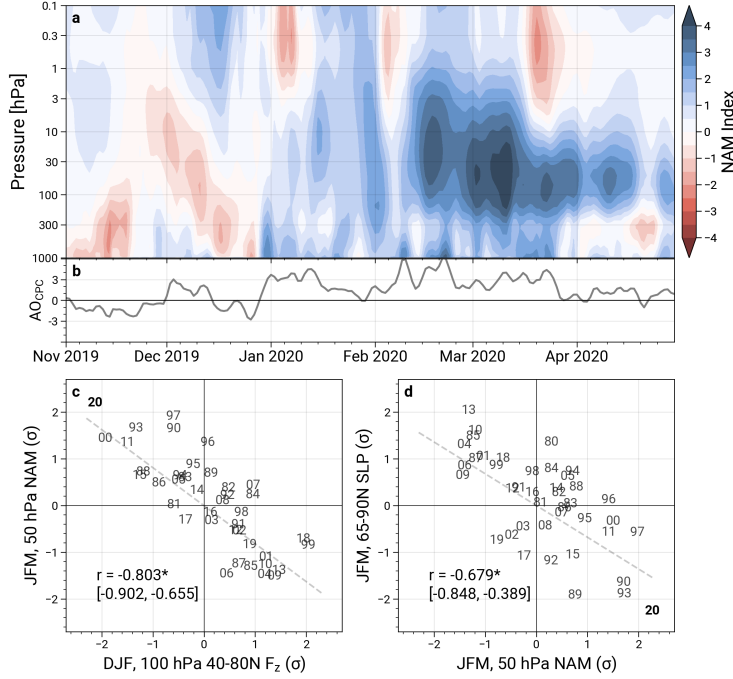


Figure 3. Time series of the Northern Annular Mode (a) and CPC Arctic Oscillation (b) indices from November 2019 through April 2020. Also shown are scatterplots of December-February (DJF) 100 hPa 40-80°N averaged vertical component of the Eliassen-Palm Flux (F_z) versus the JFM 50 hPa NAM index (c), and the JFM 50 hPa NAM index versus 65-90°N sea level pressure (d). All quantities in the scatter plots are standardized with respect to the yearly seasons. Correlations are indicated in the top left of c and d alongside 99% bootstrap confidence intervals from 50000 resamples.

275 While we have shown that the 2020 JFM NAM index was consistent with extremely
 276 low upward wave activity at 100 hPa (Fig 3c), the 100 hPa level is generally represen-
 277 tative of the lower stratosphere, and thus upward wave activity at this level is not nec-
 278 essarily indicative of wave activity from the troposphere (e.g., see discussion in de la Cámara
 279 et al., 2017). Figure 4 shows the yearly DJF mean F_z at 300 hPa in the upper tropo-
 280 sphere versus 100 hPa as a scatterplot. These are positively correlated, but only mod-
 281 estly so ($r = 0.46$), indicating that the amount of wave activity in the upper troposphere
 282 is not a perfect predictor of that for the lower stratosphere on seasonal timescales. Nonethe-
 283 less, 2019/2020 stands out among the other years as being the most coherent extreme
 284 minimum in DJF F_z at 100 and 300 hPa, indicating that low wave driving of the strato-
 285 sphere by the troposphere should have played a role in the development of the strong
 286 polar vortex in JFM.

287 At the surface, extratropical sea level pressure (SLP) anomalies were consistent with
 288 the long-lived positive AO and strong stratospheric polar vortex (Fig 3a,b,d). Figure 5a
 289 shows that the SLP anomalies were primarily characterized by an annular pattern of anom-
 290 alously low pressure in the polar cap, surrounded by a ring of anomalously high pressure
 291 in mid-latitudes, which closely resembles the canonical AO pattern. Figure 5b illustrates
 292 the 2020 JFM mean CPC AO index was the highest on record since 1950 with a value
 293 of ~ 2.7 . Moreover, the persistence of this positive AO event was unprecedented; the min-
 294 imum and maximum daily CPC AO index values during JFM 2020 were both the high-

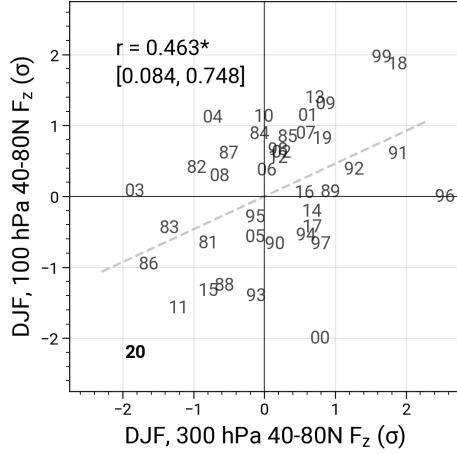


Figure 4. Scatterplot of the December-February (DJF) mean of the 40-80°N averaged vertical component of the EP-flux (F_z) at 300 hPa versus 100 hPa. The values shown are standardized with respect to the yearly seasons. The year labels are for the January of each season. The correlation is indicated in the top left alongside 99% bootstrap confidence intervals from 50000 resamples.

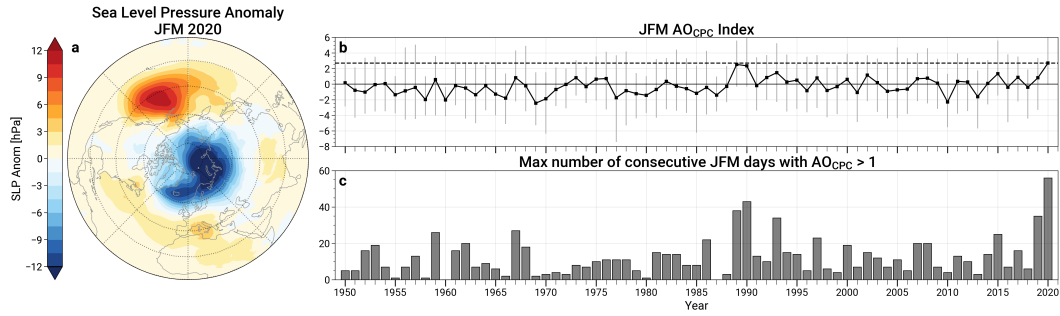


Figure 5. Map of Northern Hemisphere sea level pressure anomalies averaged over January-March (JFM) 2020 (a), yearly time series of the JFM mean CPC AO index (b), and yearly time series of the max number of consecutive JFM days in which the CPC AO index exceeded 1 (c). The whiskers in panel b represent the range of the AO values during the respective JFM seasons; the black dashed horizontal line is plotted at the mean value for 2020.

est on record, and values were consecutively above 1 for 56 days, greater than any previous year shown (Fig 5c).

The persistent positive AO during JFM 2020 was reflected in seasonal surface temperatures and precipitation. Figure 6 compares the observed seasonal patterns of surface temperature and precipitation anomalies with those that are congruent with the AO, determined from multiplying the 2020 JFM CPC AO value with the regression map of these quantities onto the JFM CPC AO historical time series. Surface temperatures were primarily characterized by very anomalous warmth in Eurasia, and cold in Canada, Greenland, and Alaska (Fig 6a). The Eurasian warmth (from 0-135°E, 45-75°N) was unprecedented in the MERRA-2 record back to 1980 (not shown). Precipitation was largely above normal in bands along Northern Europe, central Siberia, and southern Eurasia (Fig 6d).

306 The patterns congruent with the AO are generally consistent with that observed, but
 307 typically of lesser amplitude (e.g., the underestimation of temperatures over Eurasia; Fig 6b,e).
 308 Zonal means of the observed and AO-congruent anomalies (Fig 6c,f) highlight rough es-
 309 timates of the fractions of patterns attributable to the AO. Between 40 and 70°N, the
 310 JFM AO explains about 2/3 of the amplitude of temperature anomalies, with a resid-
 311 ual of about 0.5 K. The AO explains virtually all of the zonal mean precipitation anom-
 312 alies between roughly 55-70°N, but overestimates the dry band along approximately 40°N.
 313 We note these quantities are not detrended, and thus some of the observed patterns (such
 314 as the Eurasian warmth) may also be attributable to climate change warming.

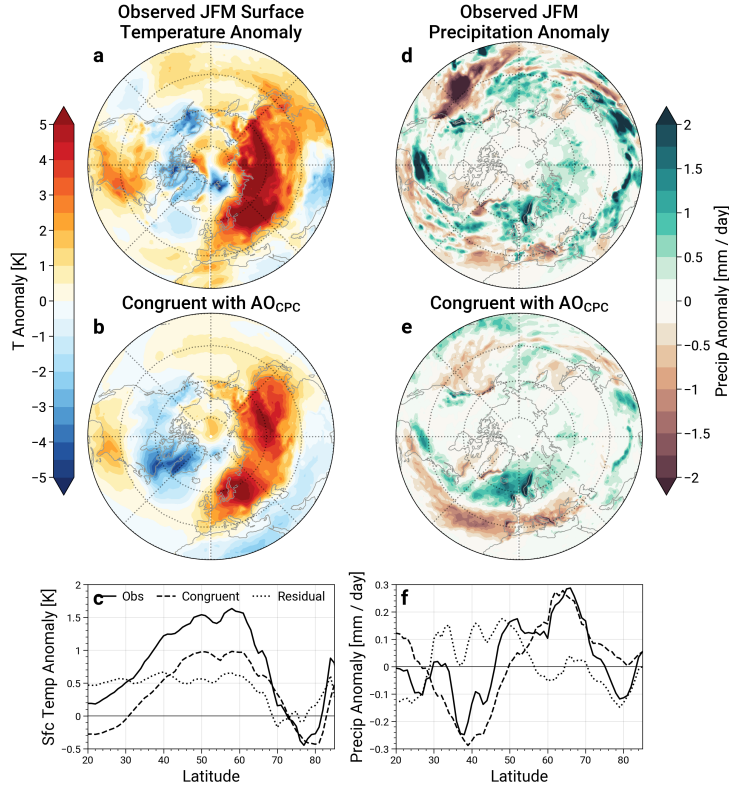


Figure 6. Maps of the observed January-March (JFM) 2020 anomalies in surface temperatures and precipitation (a,d), and the anomalies congruent with the JFM CPC AO (b,e). The last row shows the zonal means of the observed anomalies, the AO reconstruction, and the residuals (c, f).

315 **3.3 Wave Driving and Reflection: Dynamic Control of Polar Vortex Strength**

316 The occurrence of the extremely strong stratospheric polar vortex of 2020 can be
 317 partly understood through a closer examination of the seasonal evolution of tropospheric
 318 wave driving (Figure 7). In general, waves in the troposphere that linearly interfere in
 319 a constructive/destructive way with the climatological stationary wave pattern result in
 320 amplified/dampened wave driving of the polar vortex (see, e.g., Garfinkel et al., 2010;
 321 Kolstad & Charlton-Perez, 2011; Smith & Kushner, 2012). November 2019 (Fig 7a) fea-
 322 tured enhanced ridging over the Gulf of Alaska and the Ural mountains region. The pat-
 323 terns of 300 hPa geopotential height anomalies were generally constructive with the cli-
 324 matological stationary waves, which indicates enhanced wave driving occurred during
 325 this time. This is consistent with the positive anomalies in 40-80°N F_z (Fig 7f) in the

326 troposphere and stratosphere from mid to late November, which was associated with a
 327 short duration weakening event (see, e.g., Figures 1 and 3). The December geopotential
 328 height anomalies (Fig 7b) show less coherent patterns, which is consistent with the
 329 alternating periods of positive and negative F_z anomalies within the troposphere. In con-
 330 trast, January 2020 featured geopotential height anomaly patterns in a configuration that
 331 destructively interfered with the climatological stationary waves, particularly over North
 332 America and the Pacific ocean. January also had persistent anomalously low values of
 333 F_z in both the troposphere and stratosphere, indicating a prolonged period of low wave
 334 driving of the stratosphere. Geopotential height anomalies during February and March
 335 2020 (Fig 7d,e) primarily show the canonical development of the positive NAM state,
 336 with negative anomalies in the polar cap, and positive anomalies in the midlatitudes. We
 337 showed above that upward wave activity over DJF was anomalously low in the tropo-
 338 sphere and stratosphere (Figures 3 and 4). However, there are several periods through-
 339 out the extended 2019/2020 season when F_z was anomalously high, particularly in the
 340 stratosphere, such as in mid-to-late November, mid-December to early January, late Janu-
 341 ary/early February, and mid-March (Fig 7f).

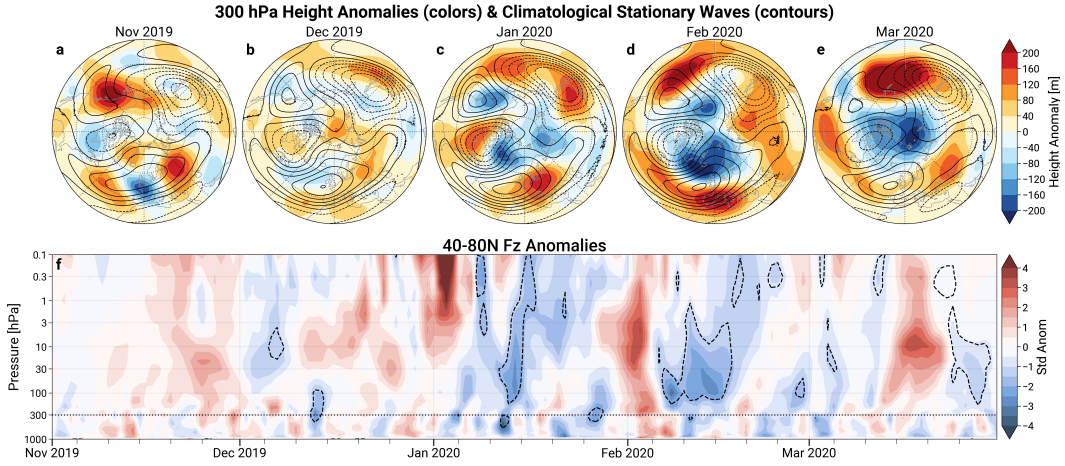


Figure 7. Maps of monthly 300 hPa geopotential height anomalies (color fill) and climatological eddy heights representing the climatological stationary waves for November 2019 – March 2020 (a - e). The bottom row (f) shows the daily time series of standardized anomalies in the 40 – 80°N average upward component of the Eliassen-Palm flux (F_z ; values are standardized using only October – March anomalies). Contours for eddy heights in the maps of a - e are plotted every 40m for values between -200 and 200m. Dashed contours in panel f show the times when the 40 – 80°N average meridional heat flux was negative.

342 Somewhat paradoxically, the transient positive F_z anomalies indicative of enhanced
 343 wave driving of the stratosphere likely played a role in promoting the robust polar vor-
 344 tex during the 2019/2020 season. The dashed contours in Figure 7f indicate when the
 345 40-80°N averaged meridional eddy heat flux was negative. The vertical component of
 346 the EP-Flux, F_z , involves a term proportional to the eddy heat flux and tends to be dom-
 347 inated by it (Andrews et al., 1987); thus the prolonged periods of negative stratospheric
 348 heat fluxes in January, February, and March were generally periods of time when wave
 349 propagation was downward as opposed to upward.

350 It is well known that wave-mean flow interactions with planetary scale waves drive
 351 wintertime polar stratospheric temperatures away from radiative equilibrium; the depo-

352 sition of easterly momentum by planetary waves establishes a meridional residual cir-
 353 culation, which drives a polar downwelling that adiabatically warms the polar strato-
 354 sphere (e.g., Andrews et al., 1987). However, total negative heat flux events like those
 355 mentioned above can have an episodic effect on the residual circulation, causing it to re-
 356 verse with upward motion in the polar cap, leading to transient adiabatic cooling of the
 357 polar stratosphere and strengthening of the polar vortex (Shaw & Perlwitz, 2013, 2014).
 358 These kinds of downward wave coupling events preferentially occur when the configu-
 359 ration of stratospheric winds support wave reflection (Perlwitz & Harnik, 2003; Harnik,
 360 2009; Shaw et al., 2010; Shaw & Perlwitz, 2013).

361 The zonal wind pattern in mid- and late winter 2020 evolved into such a reflective
 362 configuration. Figures 8a-e show monthly mean zonal mean zonal winds and EP-Flux
 363 vectors. Zonal winds in November and December (Fig 8a,b) primarily featured a single
 364 broad stratospheric jet with positive zonal wind shear over much of the extratropics. The
 365 average EP-Flux vectors during this time indicate wave propagation within the regions
 366 of strong westerlies through the stratosphere, with equatorward propagation inhibited
 367 by the regions of easterlies in the tropical stratosphere. Beginning in January and per-
 368 sisting through March (Fig 8c,d,e), a “split” jet structure emerged involving a high lat-
 369 itude jet maximum (around 60-70°N) in the lower to upper stratosphere, and a low lat-
 370 itude subtropical jet maximum (around 30-40°N) in the USLM. This configuration of
 371 the polar vortex features strong curvature of the zonal winds and negative zonal wind
 372 shear at latitudes around 60°N in the middle to upper stratosphere. This kind of con-
 373 figuration has been shown to be highly reflective with a meridional waveguide and a ver-
 374 tical “cap” beyond which wave propagation is impaired (Perlwitz & Harnik, 2003; Harnik,
 375 2009; Shaw et al., 2010).

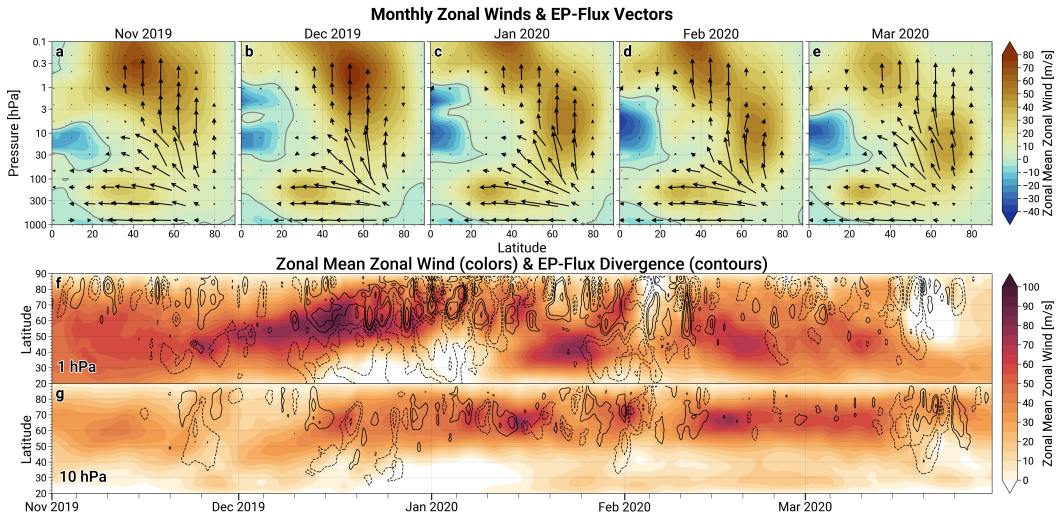


Figure 8. Latitude-pressure cross-sections of monthly mean zonal mean zonal winds and EP-flux vectors for November 2019 – March 2020 (a – e). The two bottom rows show latitude time series of zonal mean zonal winds at 1 (f) and 10 (g) hPa with contours of the acceleration by the EP-flux divergence overlaid. Only relatively extreme values of EP-flux divergence are plotted, for contours of $\pm[8, 16, 32, 64]$ m/s/day (contours for 0 m/s/day are excluded).

376 This split-jet polar vortex structure initially developed following a transient dis-
 377 turbance in early January that primarily affected the vortex within the USLM. Figure 8f,g
 378 show latitude/time series of zonal winds and acceleration by EP-Flux divergence from

379 November through March at 10 and 1 hPa. While the jet maximum at 1 hPa began the
 380 season at relatively low latitudes around 40°N, the jet maximum shifted poleward un-
 381 der wave driving before being nearly eroded away in early January. Due to the decreases
 382 in density with altitude, waves that reach the upper stratosphere tend to grow to large
 383 amplitudes and break there, resulting in a poleward movement of the vortex edge like
 384 that shown here (Dunkerton & Delisi, 1986; Dunkerton, 2000; Scott et al., 2004). How-
 385 ever, radiative time scales are short at these altitudes (e.g., Newman & Rosenfield, 1997),
 386 meaning that fast cooling under radiative relaxation can allow the rapid re-establishment
 387 of the upper stratospheric jet maximum at lower latitudes (e.g., Dunkerton & Delisi, 1985;
 388 Dunkerton, 2000). This process is consistent with the zonal wind evolution at 1 hPa (and
 389 higher altitudes; not shown) in January, and it repeated in February. The polar vortex
 390 jet at 10 hPa remained comparatively undisturbed during these times (Fig 8g) due to
 391 the transient nature of the upward wave pulses, meaning negative wind shear developed
 392 between the middle and upper stratosphere. The negative heat flux events only occurred
 393 after the re-establishment of the USLM jet at mid-latitudes (associated with the “split”
 394 in the zonal mean).

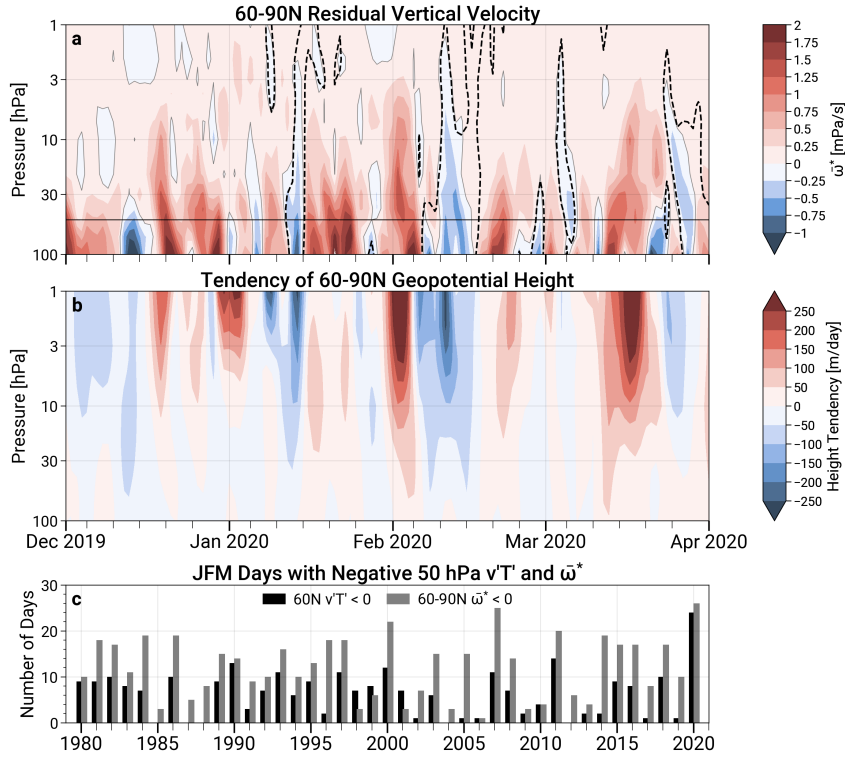


Figure 9. 60 – 90°N polar cap averaged residual vertical (pressure) velocity (a), the tendency of 60 – 90°N average geopotential heights (b), and the number of days with negative heat fluxes and a reversed residual circulation (c). The dashed contours in panel a show when the meridional eddy heat flux at 60°N was negative. Only pressure levels between 100 and 1 hPa are plotted in panels a and b. The black horizontal line in panel a corresponds to the 50 hPa level for which statistics are shown in panel c. Note that positive/negative pressure velocities indicate downward/upward motion, respectively.

395 The reflective zonal wind configuration and subsequent negative heat flux events
 396 aided in dynamically cooling and strengthening the polar vortex during the 2020 season.
 397 Figure 9 shows the 60-90°N average residual vertical pressure velocity ($\bar{\omega}^*$) and time
 398 tendencies of polar cap geopotential heights. The periods with negative heat fluxes at
 399 60°N are highlighted in Figure 9a by dashed contours. These events clearly correspond
 400 to reversals in the residual velocity that span almost the full polar stratospheric column.
 401 These events also coincide with negative polar cap height tendencies (Fig 9b), generally
 402 indicating the vortex strengthened and cooled during these events, which is consistent
 403 with prior studies (Shaw & Perlwitz, 2013, 2014). We further find that the 2020 JFM
 404 season featured the largest number of days at 50 hPa with negative heat fluxes at 60°N
 405 and with a reversed polar cap residual vertical velocity in the MERRA-2 record (Fig 9c).

406 3.4 Polar Processing and Ozone Loss

407 The extremes in two-way wave coupling contributed to developing and maintain-
 408 ing a record strong polar vortex, which contributed to record ozone loss. Here we will
 409 show how characteristics of the polar vortex and conditions within it were conducive for
 410 the chemical destruction of ozone. We examine diagnostics of polar processing, and compare
 411 with other years with strong and cold polar vortices and/or large ozone loss, includ-
 412 ing 1996/1997 (Coy et al., 1997; Manney et al., 1997; Newman et al., 1997), 2010/2011
 413 (Manney et al., 2011), and 2015/2016 (Manney & Lawrence, 2016; Matthias et al., 2016).

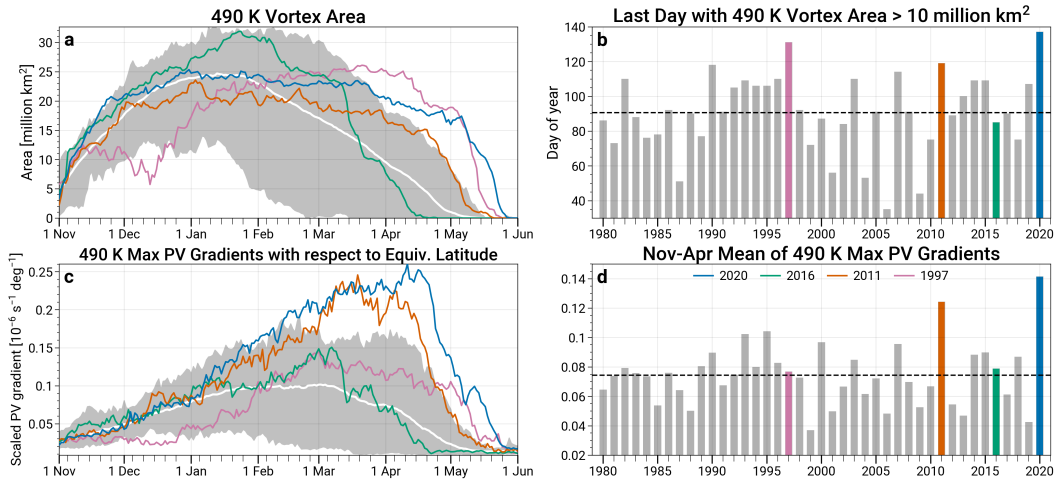


Figure 10. The left column shows daily time series of 490 K vortex area (a), and maximum PV gradients with respect to equivalent latitude (c). The right column shows derived statistics including the last day with 490 K vortex area above 10 million km² (b), and the November-March mean of the maximum PV gradients (d). The 2019/2020 season is highlighted in blue, with other relevant winters shown in green (2015/2016), orange (2010/2011) and pink (1996/1997). The grey envelopes and white lines in panels a and c represent (respectively) the climatological ranges and means after excluding the four highlighted years. The dashed horizontal lines in panels b and d represent the climatological average across the available years.

414 The 2019/2020 polar vortex was exceptionally strong and long lived in the lower
 415 stratosphere, providing a robust containment vessel for chemical processing to occur in
 416 early spring as sunlight returned. Figure 10 shows time series of vortex area and maximum
 417 potential vorticity (PV) gradients. While the 2019/2020 vortex at 490 K (around
 418 50 - 60 hPa) was larger than normal in November, it was only about average size from

419 December through January. However, the vortex remained at a roughly constant size be-
 420 tween 20-25 million km² until the beginning of April, at which point its size was among
 421 the largest on record. In the lower stratosphere, strong PV gradients are known to in-
 422 hibit mixing into and out of the vortex, and thus the magnitude of PV gradients describes
 423 how well the vortex edge acts as a barrier to transport (e.g., Hoskins et al., 1985; Jukes
 424 & McIntyre, 1987; Scott et al., 2004). Here we show PV gradients as a function of equiv-
 425 alent latitude, which describe how closely contours of PV are spaced in an equivalent area
 426 coordinate system (see, e.g., Butchart & Remsberg, 1986). The daily maximum PV gra-
 427 dients (which generally occur at the polar vortex edge) over the 2019/2020 season started
 428 out near normal but became anomalously strong beginning in January before reaching
 429 all-time record highs in February through April (Fig 10c). The size of the lower strato-
 430 spheric vortex during 2019/2020 remained above 10 million km² longer than any other
 431 previous year (Fig 10b), even 1996/1997, which had the largest vortex region from late
 432 March through the beginning of May. Similarly, the extended November-April 2020 mean
 433 maximum PV gradients were the largest in the MERRA-2 record (Fig 10d).

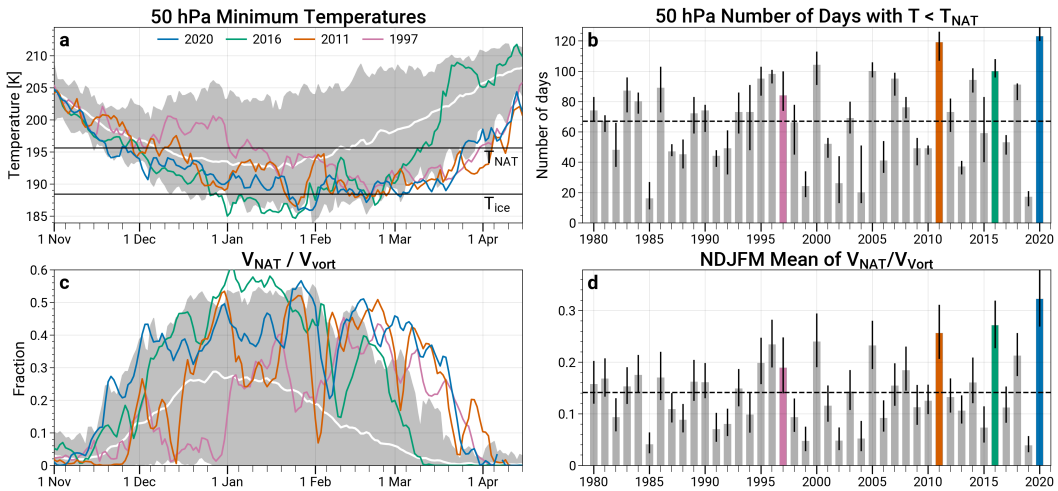


Figure 11. As in Figure 10, but the left column shows daily time series of 50 hPa minimum temperatures poleward of 40°N (a), and the volume of air in the lower stratosphere with temperatures below the nitric acid trihydrate (NAT) polar stratospheric cloud (PSC) threshold (T_{NAT}) normalized by the vortex volume (V_{NAT}/V_{vort} ; c). The right column shows yearly integrated statistics, including the total number of days with temperatures below T_{NAT} at 50 hPa, and the November-March mean V_{NAT}/V_{vort} (d). Panel a has labeled horizontal black lines that represent the approximate formation thresholds for NAT and ice PSCs. The whiskers in panels b and d represent the ranges from accounting for ± 1 K uncertainties in the specific T_{NAT} threshold.

434 The 2019/2020 polar vortex was also the coldest in the MERRA-2 record for the
 435 formation of PSCs. In Figure 11, daily minimum temperatures at 50 hPa (Figures 11a)
 436 reached some all-time record lows in late November and early December, and temper-
 437 atures remained lower than the formation threshold for nitric acid trihydrate (NAT) PSCs
 438 until approximately March 25th. While this was not the latest date on record, 2019/2020
 439 still had the largest total number of days with temperatures below T_{NAT} (Fig 11b) be-
 440 cause of the early onset of the cold period. The vortex volume fraction of lower strato-
 441 spheric air with temperatures below T_{NAT} paints a consistent picture (Fig 11c); the 2019/2020
 442 season attained all-time record maxima during some periods in mid-November and early
 443 December. Thereafter, the pool of cold air within the vortex remained relatively stable

444 between fractions of 0.4 - 0.5 until early March (except for a brief dip in early February).
 445 Figure 11d suggests that roughly a third of the vortex volume in the lower stratosphere
 446 contained temperatures conducive to the formation of PSCs in the seasonal mean, the
 447 largest in any year in the MERRA-2 record.

448 Based on the results shown here, the 2019/2020 season had the greatest ozone loss
 449 *potential* ever observed. The polar processing conditions over the 2019/2020 season most
 450 closely resembled that seen during 2010/2011, which also had a relatively constant-sized
 451 vortex until late in the season, anomalously large PV gradients, and an extensive period
 452 of low temperatures. The 2015/2016 season also had an early onset of low temperatures
 453 and still holds some records for cold, but the vortex weakened much earlier in a dynamic
 454 final warming. The 1996/1997 season was effectively delayed by a month because an early
 455 winter warming kept the vortex small, weak, and warm, meaning less time was available
 456 for polar processing to occur.

457 Column ozone amounts in late winter and early spring suggest that exceptional ozone
 458 loss did occur: Figure 12 shows the February-April (FMA) 2020 mean column ozone anom-
 459 alies alongside yearly time series of the FMA average of polar cap ($63 - 90^\circ\text{N}$) column ozone
 460 back to 1979 (the period over which regular total column ozone measurements were made
 461 by satellite instruments). Figure 12a shows that column ozone was anomalously low by
 462 more than 100 Dobson units (DU) over the pole for these three months. This ozone deficit
 463 is further reflected by the polar cap average time series shown in Figure 12b, which shows
 464 that the 2020 FMA mean was the lowest on record since 1979, with a seasonal average
 465 less than 340 DU. The interpretation of low total column ozone amounts as they relate
 466 to chemical ozone depletion requires great caution, as dynamical influences related to
 467 tropospheric weather systems, lower stratospheric cold pools, and the location of the tropopause
 468 can cumulatively help to induce low column ozone amounts on daily to seasonal timescales
 469 (e.g., see discussions in Petzoldt, 1999; Manney et al., 2011). However, the persistence
 470 of polar processing conditions conducive for chemical loss, and the persistently low col-
 471 umn ozone values point to chemical depletion in 2019/2020 being a large factor. Fur-
 472 ther, (Manney et al., submitted 2020) show evidence of chemical loss in vertically-resolved
 473 ozone profiles matching or exceeding that in 2011.

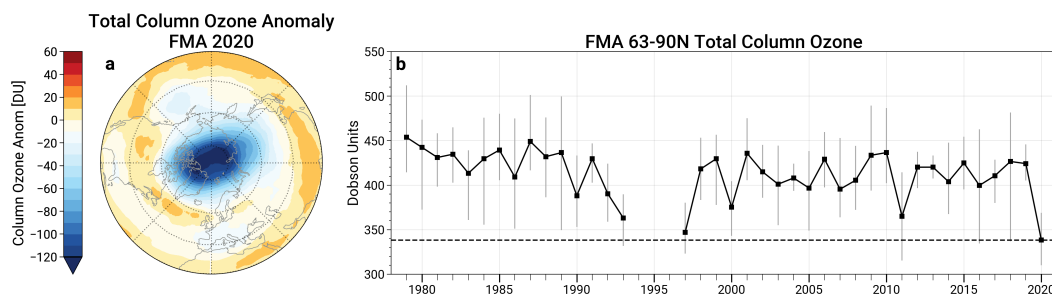


Figure 12. Map of Northern Hemisphere total column ozone anomalies averaged over February-April (FMA) 2020 (a) and yearly time series of the FMA mean $60-90^\circ\text{N}$ polar cap ozone. The whiskers in panel b represent the range of the polar cap ozone values during the respective FMA seasons; the black dashed horizontal line is plotted at the mean value for 2020. The missing data between 1994-1996 is during a period without satellite column ozone observations.

474 4 Conclusions & Discussion

475 The 2019/2020 NH stratospheric polar vortex was remarkably strong. The west-
 476 erly stratospheric circulation represented by the polar vortex was the strongest on record
 477 for December-March winter seasons back to 1979/1980; if considering earlier years back
 478 to 1958/1959 for which data are more uncertain, 2019/2020 ranks among the top three,
 479 although it depends on the specific level under consideration (e.g., 2019/2020 remains
 480 the strongest at 100 hPa). The robust polar vortex appears to have developed due to
 481 a combination of weak tropospheric wave driving and a series of downward wave cou-
 482 pling events that occurred following the development of a reflective configuration of the
 483 polar vortex. Numerous aspects of the 2019/2020 winter and early spring were record
 484 breaking, and involved extremes in two-way troposphere-stratosphere coupling.

485 The positive AO and positive stratospheric NAM developed as a coherent event
 486 spanning the troposphere and stratosphere. As a result, the direction of causality be-
 487 tween the strongly positive NAM in the stratosphere and strongly positive AO in the
 488 troposphere is somewhat unclear. However, the persistence of the exceptionally strong
 489 vortex throughout the stratosphere suggests a stratospheric influence on the AO is more
 490 likely. The January-March 2020 mean AO was the largest on record and persistently pos-
 491 itive. Large fractions of the observed surface temperature and precipitation anomalies
 492 in JFM were consistent with this large amplitude AO event.

493 The strong and long-lived polar vortex also provided ideal conditions for chemi-
 494 cal ozone destruction to take place. In the lower stratosphere, the polar vortex was a ro-
 495 bust transport barrier and very long lived, which isolated Arctic air during the key tran-
 496 sition period out of polar night. Furthermore, temperatures low enough to form polar
 497 stratospheric clouds within the vortex developed early in the season, and on average en-
 498 closed about a third of the vortex volume. In total, the number of days with such low
 499 temperatures exceeded 4 months. These conditions are unprecedented back to 1979/1980,
 500 making 2019/2020 the season with the greatest ozone loss potential on record. Polar cap
 501 column ozone amounts subsequently reached low levels never before observed in the Arc-
 502 tic at this time of year.

503 We have focused on the unusual 2019/2020 polar vortex, and how it related to the
 504 observed climate extremes in the Arctic Oscillation and stratospheric ozone. Our results
 505 particularly highlight the important confluence of tropospheric and stratospheric con-
 506 ditions that overall made the exceptional polar vortex, AO, and ozone depletion possi-
 507 ble. Further studies are necessary to fill in the gaps related to detailed mechanisms, ob-
 508 servations, predictability, and the full extent of impacts. Below we pose research ques-
 509 tions motivated by the present work.

510 1. *What were the drivers (if any) of the strong vortex and/or AO events over internal*
 511 *variability?*

512 Interannual variability of the Arctic polar vortex is influenced by a variety of back-
 513 ground climate forcings and boundary conditions that act on sub-seasonal to seasonal
 514 timescales. These “drivers” impact the generation of waves in the troposphere, or influ-
 515 ence how they propagate through the atmosphere. Detailed modeling and attribution
 516 studies will be necessary to determine whether such processes played a role in the de-
 517 velopment of the strong polar vortex and/or the AO event over simple internal variabil-
 518 ity.

519 For example, sea surface temperatures (SSTs) in various regions have been linked
 520 to seasonal variability in the Arctic polar vortex. Some studies tied the previous strong
 521 and cold springtime polar vortices of 1997 and 2011 to positive SST anomalies in the north
 522 central Pacific (Hurwitz et al., 2011, 2012); more generally, SSTs in this region have been
 523 shown to modulate tropospheric planetary wave activity and the strength of the vortex
 524 (e.g., Hu et al., 2018; Xie et al., 2020). Positive SST anomalies in the Indian Ocean have

525 also been shown to encourage a strengthened Arctic polar vortex and positive NAM in
 526 the troposphere (Hoerling & Kumar, 2002; Hoerling et al., 2004; Li et al., 2010; Fletcher
 527 & Kushner, 2011), particularly in isolation from impacts by the El Niño-Southern Os-
 528 cillation (ENSO) (Fletcher & Cassou, 2015). It is worth noting that the boreal autumn
 529 of 2019 featured a record strong Indian Ocean dipole event (see, e.g., Johnson, 2020) and
 530 warm north Pacific SSTs from a marine heatwave (see, e.g., L’Heureux, 2019), amidst
 531 largely neutral ENSO conditions. Other background forcings and boundary conditions
 532 that have been shown to impact the polar vortex include the tropical stratospheric quasi-
 533 biennial oscillation (e.g., Baldwin et al., 2001; Garfinkel, Shaw, et al., 2012; White et al.,
 534 2016; Lu et al., 2020), and the tropical tropospheric Madden-Julian oscillation (e.g., Garfinkel,
 535 Feldstein, et al., 2012; Garfinkel et al., 2014; Liu et al., 2014; Lee et al., 2019).

536 *2. How well were the strong polar vortex and AO events predicted by sub-seasonal to sea-
 537 sonal forecast models, and did the stratosphere contribute to tropospheric forecast skill?*

538 It is possible that some fraction of skill in sub-seasonal to seasonal (S2S) forecasts
 539 during the 2019/2020 winter and spring could be related to skill in predicting the strong
 540 polar vortex event, or being initialized with it. Studies have consistently shown a rela-
 541 tionship between wintertime polar stratospheric initial conditions and improved S2S fore-
 542 cast skill (e.g., Sigmond et al., 2013; Tripathi, Baldwin, et al., 2015; Tripathi, Charlton-
 543 Perez, et al., 2015; Scaife et al., 2016; Nie et al., 2019). Recent work suggests there is
 544 also a relationship between model skill in predicting the stratosphere and skill for the
 545 troposphere (e.g., Domeisen et al., 2020a, 2020b). A more complete accounting of the
 546 impacts related to stratosphere-troposphere coupling is also warranted: the reflective state
 547 of the stratosphere and multiple downward wave coupling events may have had a direct
 548 influence on tropospheric weather and circulation during the 2019/2020 winter and early
 549 spring. Downward wave reflection events have themselves been shown to initiate posi-
 550 tive phases of the North Atlantic Oscillation (Shaw & Perlwitz, 2013) and weather events
 551 such as North Pacific blocking and cold spells in North America and Eurasia (Kodera
 552 et al., 2008; Kodera & Mukougawa, 2017; Matthias & Kretschmer, 2020).

553 *3. What were the relative roles of dynamical transport versus chemical loss processes in
 554 determining the low early spring column ozone?*

555 The anomalous polar cap ozone during the late winter and early spring of 2020 was
 556 clearly record breaking. The low ozone is generally consistent with the persistently strong
 557 polar vortex, which would have led to depressed ozone amounts due to a weakened resid-
 558 ual circulation, and enhanced chemical loss due to the persistently cold polar vortex (Tegtmeier
 559 et al., 2008; Shaw & Perlwitz, 2014; Lubis et al., 2017). In 2010/2011 (the winter pre-
 560 viously having the most extreme ozone loss) the individual contributions from transport
 561 and chemical loss were both found to be record breaking based on a mixture of obser-
 562 vations and models (e.g., Balis et al., 2011; Manney et al., 2011; Sinnhuber et al., 2011;
 563 Adams et al., 2012; Strahan et al., 2013; Griffin et al., 2019). It will similarly be nec-
 564 essary for studies to utilize a variety of observations and models to determine the rel-
 565 ative roles of dynamical versus chemical impacts on low column ozone in spring 2020,
 566 in addition to providing quantitative vertically-resolved chemical loss estimates. For ex-
 567 ample, Manney et al. (submitted 2020, submitted for this special collection) use obser-
 568 vations of relevant chemical species from the Aura Microwave Limb Sounder to illustrate
 569 the processes leading to exceptional chemical ozone loss by spring 2020.

570 *4. Were there downstream impacts related to the strong vortex, ozone deficit, and per-
 571 sistent positive tropospheric AO events?*

572 The strong polar vortex, low ozone, and positive AO events that occurred in the
 573 late winter/early spring of 2020 were each record breaking on seasonal timescales, and
 574 as a result, there is a possibility they had farther-reaching consequences. For example,
 575 it is possible that the depleted ozone into spring 2020 may have helped to maintain the

576 positive AO through April. One modeling study has shown that negative Arctic ozone
577 anomalies can cause a feedback on the strength of the vortex that increases the prob-
578 ability of a positive tropospheric AO (Karpechko et al., 2014), in a similar manner to
579 the observed tropospheric impacts of the Antarctic ozone hole (Thompson & Solomon,
580 2002; Shindell & Schmidt, 2004; Thompson et al., 2011). This kind of relationship be-
581 tween stratospheric ozone and the tropospheric circulation underpins why recent stud-
582 ies have suggested that springtime Arctic stratospheric ozone anomalies are linked with
583 surface temperatures and precipitation in specific regions for weeks to months ahead (e.g.,
584 Calvo et al., 2015; Ivy et al., 2017; Xie et al., 2018; Stone et al., 2019; Wang et al., 2020).

585 Additional climatologically relevant impacts are also possible: One recent study
586 illustrated that springtime stratospheric ozone intrusions are strongly impacted by the
587 abundance of ozone in the lowermost stratosphere in early spring (Albers et al., 2018),
588 meaning there could be a signature of the 2020 low ozone event in subsequent ozone in-
589 trusions of spring 2020. Another recent study has shown a relationship between a posi-
590 tive AO in the winter and early spring and increased fire activity and burn area in south-
591 eastern Siberia, a region where carbon release by fires can accelerate Arctic warming (Kim
592 et al., 2020). Yet another recent study has found a link between the timing of the spring-
593 time Arctic polar vortex breakdown and the distribution of sea ice thickness anomalies
594 all the way until the following autumn (Kelleher et al., 2020). Further study will be re-
595 quired to determine whether responses consistent with the above mentioned relationships,
596 or other events, arise due to influences from the exceptional 2019/2020 winter and spring.

597 These and other questions will be the focus of further work; we expect that many
598 will be addressed in the Journal of Geophysical Research/Geophysical Research Letters
599 Special Collection on the exceptional 2019/2020 Arctic polar vortex in which this arti-
600 cle appears.

601 **Acknowledgments**

602 We thank John Albers for providing comments on an early version of the manuscript.
603 We also thank the Microwave Limb Sounder team for computational support related to
604 calculating the polar processing diagnostics. ZDL and JP acknowledge support from Fed-
605 erally Appropriated Funds. The datasets used herein are publicly available. NASA MERRA-
606 2 data are available from NASA’s GES DISC at [https://disc.gsfc.nasa.gov/datasets](https://disc.gsfc.nasa.gov/datasets?keywords=MERRA-2)
607 [?keywords=MERRA-2](https://disc.gsfc.nasa.gov/datasets?keywords=MERRA-2). JRA-55 data are available from the NCAR Research Data Archive
608 at <https://rda.ucar.edu/datasets/ds628.0/>. The CPC AO index is kept up to date
609 at [ftp://ftp.cpc.ncep.noaa.gov/cwlinks/norm.daily.ao.index.b500101.current](ftp://ftp.cpc.ncep.noaa.gov/cwlinks/norm.daily.ao.index.b500101.current.ascii)
610 [.ascii](ftp://ftp.cpc.ncep.noaa.gov/cwlinks/norm.daily.ao.index.b500101.current.ascii). Ozone data and statistics from OMPS and other instruments are compiled and
611 made available via NASA’s OzoneWatch resource at [https://ozonewatch.gsfc.nasa](https://ozonewatch.gsfc.nasa.gov/)
612 [.gov/](https://ozonewatch.gsfc.nasa.gov/).

References

- 613
614 Adams, C., Strong, K., Zhao, X., Bassford, M. R., Chipperfield, M. P., Daffer, W.,
615 ... Walker, K. A. (2012). Severe 2011 ozone depletion assessed with 11 years
616 of ozone, NO₂, and OClO measurements at 80N. *Geophysical Research Letters*,
617 *39*(5). doi: 10.1029/2011GL050478
- 618 Albers, J. R., Perlwitz, J., Butler, A. H., Birner, T., Kiladis, G. N., Lawrence,
619 Z. D., ... Dias, J. (2018). Mechanisms Governing Interannual Variability
620 of Stratosphere-to-Troposphere Ozone Transport. *Journal of Geophysical*
621 *Research: Atmospheres*, *123*(1), 234–260. doi: 10.1002/2017JD026890
- 622 Andrews, D. G., Leovy, C. B., & Holton, J. R. (1987). *Middle Atmosphere Dynam-*
623 *ics*. Academic Press.
- 624 Baldwin, M. P. (2001). Annular modes in global daily surface pressure. *Geophysical*
625 *Research Letters*, *28*(21), 4115–4118. doi: 10.1029/2001GL013564
- 626 Baldwin, M. P., & Dunkerton, T. J. (2001). Stratospheric Harbingers of Anomalous
627 Weather Regimes. *Science*, *294*(5542), 581–584. doi: 10.1126/science.1063315
- 628 Baldwin, M. P., Gray, L. J., Dunkerton, T. J., Hamilton, K., Haynes, P. H., Randel,
629 W. J., ... Takahashi, M. (2001). The quasi-biennial oscillation. *Reviews of*
630 *Geophysics*, *39*(2), 179–229. doi: 10.1029/1999RG000073
- 631 Baldwin, M. P., & Thompson, D. W. J. (2009). A critical comparison of strato-
632 sphere–troposphere coupling indices. *Quarterly Journal of the Royal Meteorolo-*
633 *gical Society*, *135*(644), 1661–1672. doi: 10.1002/qj.479
- 634 Balis, D., Isaksen, I. S. A., Zerefos, C., Zyrichidou, I., Eleftheratos, K., Tourpali, K.,
635 ... Orsolini, Y. (2011). Observed and modelled record ozone decline over the
636 Arctic during winter/spring 2011. *Geophysical Research Letters*, *38*(23). doi:
637 10.1029/2011GL049259
- 638 Black, R. X., McDaniel, B. A., & Robinson, W. A. (2006). Strato-
639 sphere–Troposphere Coupling during Spring Onset. *Journal of Climate*,
640 *19*(19), 4891–4901. doi: 10.1175/JCLI3907.1
- 641 Butchart, N., & Remsberg, E. E. (1986). The Area of the Stratospheric Polar Vor-
642 tex as a Diagnostic for Tracer Transport on an Isentropic Surface. *Journal of*
643 *the Atmospheric Sciences*, *43*(13), 1319–1339. doi: 10.1175/1520-0469(1986)
644 043(1319:TAOTSP)2.0.CO;2
- 645 Butler, A. H., Charlton-Perez, A., Domeisen, D. I. V., Garfinkel, C., Gerber,
646 E. P., Hitchcock, P., ... Son, S.-W. (2019). Chapter 11 - Sub-seasonal
647 Predictability and the Stratosphere. In A. W. Robertson & F. Vitart
648 (Eds.), *Sub-Seasonal to Seasonal Prediction* (pp. 223–241). Elsevier. doi:
649 10.1016/B978-0-12-811714-9.00011-5
- 650 Butler, A. H., Sjöberg, J. P., Seidel, D. J., & Rosenlof, K. H. (2017). A sudden
651 stratospheric warming compendium. *Earth System Science Data*, *9*(1), 63–76.
652 doi: 10.5194/essd-9-63-2017
- 653 Calvo, N., Polvani, L. M., & Solomon, S. (2015). On the surface impact of Arctic
654 stratospheric ozone extremes. *Environmental Research Letters*, *10*(9), 094003.
655 doi: 10.1088/1748-9326/10/9/094003
- 656 Charlton-Perez, A. J., Ferranti, L., & Lee, R. W. (2018). The influence of the strato-
657 spheric state on North Atlantic weather regimes. *Quarterly Journal of the*
658 *Royal Meteorological Society*, *144*(713), 1140–1151. doi: 10.1002/qj.3280
- 659 Charney, J. G., & Drazin, P. G. (1961). Propagation of planetary-scale distur-
660 bances from the lower into the upper atmosphere. *Journal of Geophysical Re-*
661 *search (1896-1977)*, *66*(1), 83–109. doi: 10.1029/JZ066i001p00083
- 662 Cohen, J., Salstein, D., & Saito, K. (2002). A dynamical framework to understand
663 and predict the major Northern Hemisphere mode. *Geophysical Research Let-*
664 *ters*, *29*(10), 51-1-51-4. doi: 10.1029/2001GL014117
- 665 Coy, L., Nash, E. R., & Newman, P. A. (1997). Meteorology of the polar vortex:
666 Spring 1997. *Geophysical Research Letters*, *24*(22), 2693–2696. doi: 10.1029/
667 97GL52832

- 668 de la Cámara, A., Albers, J. R., Birner, T., Garcia, R. R., Hitchcock, P., Kinnison,
669 D. E., & Smith, A. K. (2017). Sensitivity of Sudden Stratospheric Warmings
670 to Previous Stratospheric Conditions. *Journal of the Atmospheric Sciences*,
671 *74*(9), 2857–2877. doi: 10.1175/JAS-D-17-0136.1
- 672 Domeisen, D. I. V. (2019). Estimating the Frequency of Sudden Stratospheric
673 Warming Events From Surface Observations of the North Atlantic Oscilla-
674 tion. *Journal of Geophysical Research: Atmospheres*, *124*(6), 3180–3194. doi:
675 10.1029/2018JD030077
- 676 Domeisen, D. I. V., Butler, A. H., Charlton-Perez, A. J., Ayarzagüena, B., Bald-
677 win, M. P., Dunn-Sigouin, E., . . . Taguchi, M. (2020a). The Role of the
678 Stratosphere in Subseasonal to Seasonal Prediction: 1. Predictability of
679 the Stratosphere. *Journal of Geophysical Research: Atmospheres*, *125*(2),
680 e2019JD030920. doi: 10.1029/2019JD030920
- 681 Domeisen, D. I. V., Butler, A. H., Charlton-Perez, A. J., Ayarzagüena, B., Bald-
682 win, M. P., Dunn-Sigouin, E., . . . Taguchi, M. (2020b). The Role of the
683 Stratosphere in Subseasonal to Seasonal Prediction: 2. Predictability Arising
684 From Stratosphere-Troposphere Coupling. *Journal of Geophysical Research:*
685 *Atmospheres*, *125*(2), e2019JD030923. doi: 10.1029/2019JD030923
- 686 Dunkerton, T. J. (2000). Midwinter Deceleration of the Subtropical Meso-
687 spheric Jet and Interannual Variability of the High-Latitude Flow in UKMO
688 Analyses. *Journal of the Atmospheric Sciences*, *57*(23), 3838–3855. doi:
689 10.1175/1520-0469(2000)057<3838:MDOTSM>2.0.CO;2
- 690 Dunkerton, T. J., & Delisi, D. P. (1985). The subtropical mesospheric jet ob-
691 served by the Nimbus 7 Limb Infrared Monitor of the Stratosphere. *Jour-*
692 *nal of Geophysical Research: Atmospheres*, *90*(D6), 10681–10692. doi:
693 10.1029/JD090iD06p10681
- 694 Dunkerton, T. J., & Delisi, D. P. (1986). Evolution of potential vorticity in the win-
695 ter stratosphere of January-February 1979. *Journal of Geophysical Research:*
696 *Atmospheres*, *91*(D1), 1199–1208. doi: 10.1029/JD091iD01p01199
- 697 Dunn-Sigouin, E., & Shaw, T. A. (2015). Comparing and contrasting extreme
698 stratospheric events, including their coupling to the tropospheric circula-
699 tion. *Journal of Geophysical Research: Atmospheres*, *120*(4), 1374–1390. doi:
700 10.1002/2014JD022116
- 701 Fletcher, C. G., & Cassou, C. (2015). The Dynamical Influence of Separate Telecon-
702 nections from the Pacific and Indian Oceans on the Northern Annular Mode.
703 *Journal of Climate*, *28*(20), 7985–8002. doi: 10.1175/JCLI-D-14-00839.1
- 704 Fletcher, C. G., & Kushner, P. J. (2011). The Role of Linear Interference in the
705 Annular Mode Response to Tropical SST Forcing. *Journal of Climate*, *24*(3),
706 778–794. doi: 10.1175/2010JCLI3735.1
- 707 Garfinkel, C. I., Benedict, J. J., & Maloney, E. D. (2014). Impact of the MJO
708 on the boreal winter extratropical circulation. *Geophysical Research Letters*,
709 6055–6062. doi: 10.1002/2014GL061094@10.1002/(ISSN)1944-8007.ATMOS
710 _VARIABILITY
- 711 Garfinkel, C. I., Feldstein, S. B., Waugh, D. W., Yoo, C., & Lee, S. (2012). Observed
712 connection between stratospheric sudden warmings and the Madden-Julian Os-
713 cillation. *Geophysical Research Letters*, *39*(18). doi: 10.1029/2012GL053144
- 714 Garfinkel, C. I., Hartmann, D. L., & Sassi, F. (2010). Tropospheric Precursors of
715 Anomalous Northern Hemisphere Stratospheric Polar Vortices. *Journal of Cli-*
716 *mate*, *23*(12), 3282–3299. doi: 10.1175/2010JCLI3010.1
- 717 Garfinkel, C. I., Shaw, T. A., Hartmann, D. L., & Waugh, D. W. (2012). Does the
718 Holton–Tan Mechanism Explain How the Quasi-Biennial Oscillation Modu-
719 lates the Arctic Polar Vortex? *Journal of the Atmospheric Sciences*, *69*(5),
720 1713–1733. doi: 10.1175/JAS-D-11-0209.1
- 721 Gelaro, R., McCarty, W., Suárez, M. J., Todling, R., Molod, A., Takacs, L., . . .
722 Zhao, B. (2017). The Modern-Era Retrospective Analysis for Research and

- 723 Applications, Version 2 (MERRA-2). *Journal of Climate*, 30(14), 5419–5454.
724 doi: 10.1175/JCLI-D-16-0758.1
- 725 GMAO. (2020a). *MERRA-2 inst3_3d_asm_Np: 3d, 3-Hourly, Instantaneous, Pressure-*
726 *Level, Assimilation, Assimilated Meteorological Fields V5.12.4*. doi: 10.5067/
727 QBZ6MG944HW0,
- 728 GMAO. (2020b). *MERRA-2 inst3_3d_asm_Nv: 3d, 3-Hourly, Instantaneous, Model-*
729 *Level, Assimilation, Assimilated Meteorological Fields V5.12.4*. doi: 10.5067/
730 WWQXSXQ8IVFW8
- 731 Griffin, D., Walker, K. A., Wohltmann, I., Dhomse, S. S., Rex, M., Chipperfield,
732 M. P., ... Tarasick, D. (2019). Stratospheric ozone loss in the Arctic winters
733 between 2005 and 2013 derived with ACE-FTS measurements. *Atmospheric*
734 *Chemistry and Physics*, 19(1), 577–601. doi: 10.5194/acp-19-577-2019
- 735 Harnik, N. (2009). Observed stratospheric downward reflection and its relation to
736 upward pulses of wave activity. *Journal of Geophysical Research: Atmospheres*,
737 114(D8). doi: 10.1029/2008JD010493
- 738 Hitchcock, P. (2019). On the value of reanalyses prior to 1979 for dynamical stud-
739 ies of stratosphere–troposphere coupling. *Atmospheric Chemistry and Physics*,
740 19(5), 2749–2764. doi: 10.5194/acp-19-2749-2019
- 741 Hitchcock, P., & Shepherd, T. G. (2013). Zonal-Mean Dynamics of Extended Re-
742 coveries from Stratospheric Sudden Warmings. *Journal of the Atmospheric Sci-*
743 *ences*, 70(2), 688–707. doi: 10.1175/JAS-D-12-0111.1
- 744 Hitchcock, P., Shepherd, T. G., & Manney, G. L. (2013). Statistical Characterization
745 of Arctic Polar-Night Jet Oscillation Events. *Journal of Climate*, 26(6), 2096–
746 2116. doi: 10.1175/JCLI-D-12-00202.1
- 747 Hoerling, M. P., Hurrell, J. W., Xu, T., Bates, G. T., & Phillips, A. S. (2004).
748 Twentieth century North Atlantic climate change. Part II: Understanding the
749 effect of Indian Ocean warming. *Climate Dynamics*, 23(3), 391–405. doi:
750 10.1007/s00382-004-0433-x
- 751 Hoerling, M. P., & Kumar, A. (2002). Atmospheric Response Patterns Associated
752 with Tropical Forcing. *Journal of Climate*, 15(16), 2184–2203. doi: 10.1175/
753 1520-0442(2002)015<2184:ARPAWT>2.0.CO;2
- 754 Hoskins, B. J., McIntyre, M. E., & Robertson, A. W. (1985). On the use and sig-
755 nificance of isentropic potential vorticity maps. *Quarterly Journal of the Royal*
756 *Meteorological Society*, 111(470), 877–946. doi: 10.1002/qj.49711147002
- 757 Hu, D., Guan, Z., Tian, W., & Ren, R. (2018). Recent strengthening of the strato-
758 spheric Arctic vortex response to warming in the central North Pacific. *Nature*
759 *Communications*, 9(1), 1–10. doi: 10.1038/s41467-018-04138-3
- 760 Hurwitz, M. M., Newman, P. A., & Garfinkel, C. I. (2011). The Arctic vortex in
761 March 2011: A dynamical perspective. *Atmospheric Chemistry and Physics*,
762 11(22), 11447–11453. doi: 10.5194/acp-11-11447-2011
- 763 Hurwitz, M. M., Newman, P. A., & Garfinkel, C. I. (2012). On the influence of
764 North Pacific sea surface temperature on the Arctic winter climate. *Journal of*
765 *Geophysical Research: Atmospheres*, 117(D19). doi: 10.1029/2012JD017819
- 766 Ivy, D. J., Solomon, S., Calvo, N., & Thompson, D. W. J. (2017). Observed
767 connections of Arctic stratospheric ozone extremes to Northern Hemisphere
768 surface climate. *Environmental Research Letters*, 12(2), 024004. doi:
769 10.1088/1748-9326/aa57a4
- 770 Johnson, N. (2020). *Meet ENSO’s neighbor, the Indian Ocean Dipole*.
771 [https://www.climate.gov/news-features/blogs/enso/meet-enso%E2%80%99s-](https://www.climate.gov/news-features/blogs/enso/meet-enso%E2%80%99s-neighbor-indian-ocean-dipole)
772 [neighbor-indian-ocean-dipole](https://www.climate.gov/news-features/blogs/enso/meet-enso%E2%80%99s-neighbor-indian-ocean-dipole).
- 773 Jukes, M. N., & McIntyre, M. E. (1987). A high-resolution one-layer model of
774 breaking planetary waves in the stratosphere. *Nature*, 328(6131), 590–596. doi:
775 10.1038/328590a0
- 776 Karpechko, A. Y., Hitchcock, P., Peters, D. H. W., & Schneidereit, A. (2017). Pre-
777 dictability of downward propagation of major sudden stratospheric warmings.

- 778 *Quarterly Journal of the Royal Meteorological Society*, 143(704), 1459–1470.
779 doi: 10.1002/qj.3017
- 780 Karpechko, A. Y., Perlwitz, J., & Manzini, E. (2014). A model study of tropospheric
781 impacts of the Arctic ozone depletion 2011. *Journal of Geophysical Research:
782 Atmospheres*, 119(13), 7999–8014. doi: 10.1002/2013JD021350
- 783 Kelleher, M. E., Ayarzagüena, B., & Screen, J. A. (2020). Interseasonal Connections
784 between the Timing of the Stratospheric Final Warming and Arctic Sea Ice.
785 *Journal of Climate*, 33(8), 3079–3092. doi: 10.1175/JCLI-D-19-0064.1
- 786 Kidston, J., Scaife, A. A., Hardiman, S. C., Mitchell, D. M., Butchart, N., Bald-
787 win, M. P., & Gray, L. J. (2015). Stratospheric influence on tropospheric jet
788 streams, storm tracks and surface weather. *Nature Geoscience*, 8(6), 433–440.
789 doi: 10.1038/ngeo2424
- 790 Kim, J.-S., Kug, J.-S., Jeong, S.-J., Park, H., & Schaepman-Strub, G. (2020). Ex-
791 tensive fires in southeastern Siberian permafrost linked to preceding Arctic
792 Oscillation. *Science Advances*, 6(2), eaax3308. doi: 10.1126/sciadv.aax3308
- 793 King, A. D., Butler, A. H., Jucker, M., Earl, N. O., & Rudeva, I. (2019). Observed
794 Relationships Between Sudden Stratospheric Warmings and European Climate
795 Extremes. *Journal of Geophysical Research: Atmospheres*, 124(24), 13943–
796 13961. doi: 10.1029/2019JD030480
- 797 Kobayashi, S., Ota, Y., Harada, Y., Ebata, A., Moriya, M., Onoda, H., . . . Taka-
798 hashi, K. (2015). The JRA-55 Reanalysis: General Specifications and Basic
799 Characteristics. . 2, 93(1), 5–48. doi: 10.2151/jmsj.2015-001
- 800 Kodera, K., & Mukougawa, H. (2017). Eurasian Cold Surges Triggered by the Non-
801 linear Reflection of Stratospheric Planetary Waves in December 2012. *Sola*, 13,
802 140–145. doi: 10.2151/sola.2017-026
- 803 Kodera, K., Mukougawa, H., & Itoh, S. (2008). Tropospheric impact of reflected
804 planetary waves from the stratosphere. *Geophysical Research Letters*, 35(16).
805 doi: 10.1029/2008GL034575
- 806 Kolstad, E. W., & Charlton-Perez, A. J. (2011). Observed and simulated precursors
807 of stratospheric polar vortex anomalies in the Northern Hemisphere. *Cli-
808 mate Dynamics*, 37(7), 1443–1456. doi: 10.1007/s00382-010-0919-7
- 809 Lawrence, Z. D., & Manney, G. L. (2018). Characterizing Stratospheric Polar Vor-
810 tex Variability With Computer Vision Techniques. *Journal of Geophysical Re-
811 search: Atmospheres*, 123(3), 1510–1535. doi: 10.1002/2017JD027556
- 812 Lawrence, Z. D., Manney, G. L., & Wargan, K. (2018). Reanalysis intercompar-
813 isons of stratospheric polar processing diagnostics. *Atmospheric Chemistry and
814 Physics*, 18(18), 13547–13579. doi: 10.5194/acp-18-13547-2018
- 815 Lee, R. W., Woolnough, S. J., Charlton-Perez, A. J., & Vitart, F. (2019). ENSO
816 Modulation of MJO Teleconnections to the North Atlantic and Europe. *Geo-
817 physical Research Letters*, 46(22), 13535–13545. doi: 10.1029/2019GL084683
- 818 L’Heureux, M. (2019). *Seeing Red Across the North Pacific Ocean*.
819 [https://www.climate.gov/news-features/blogs/enso/seeing-red-across-north-
820 pacific-ocean](https://www.climate.gov/news-features/blogs/enso/seeing-red-across-north-pacific-ocean).
- 821 Li, S., Perlwitz, J., Hoerling, M. P., & Chen, X. (2010). Opposite Annular Responses
822 of the Northern and Southern Hemispheres to Indian Ocean Warming. *Journal
823 of Climate*, 23(13), 3720–3738. doi: 10.1175/2010JCLI3410.1
- 824 Limpasuvan, V., Hartmann, D. L., Thompson, D. W. J., Jeev, K., & Yung, Y. L.
825 (2005). Stratosphere-troposphere evolution during polar vortex intensi-
826 fication. *Journal of Geophysical Research: Atmospheres*, 110(D24). doi:
827 10.1029/2005JD006302
- 828 Liu, C., Tian, B., Li, K.-F., Manney, G. L., Livesey, N. J., Yung, Y. L., & Waliser,
829 D. E. (2014). Northern Hemisphere mid-winter vortex-displacement and
830 vortex-split stratospheric sudden warmings: Influence of the Madden-Julian
831 Oscillation and Quasi-Biennial Oscillation. *Journal of Geophysical Research:
832 Atmospheres*, 119(22), 12,599–12,620. doi: 10.1002/2014JD021876

- 833 Lu, H., Hitchman, M. H., Gray, L. J., Anstey, J. A., & Osprey, S. M. (2020). On the
834 role of Rossby wave breaking in the quasi-biennial modulation of the strato-
835 spheric polar vortex during boreal winter. *Quarterly Journal of the Royal*
836 *Meteorological Society*, *n/a*(n/a). doi: 10.1002/qj.3775
- 837 Lubis, S. W., Silverman, V., Matthes, K., Harnik, N., Omrani, N.-E., & Wahl, S.
838 (2017). How does downward planetary wave coupling affect polar stratospheric
839 ozone in the Arctic winter stratosphere? *Atmospheric Chemistry and Physics*,
840 *17*(3), 2437–2458. doi: 10.5194/acp-17-2437-2017
- 841 Manney, G. L., Froidevaux, L., Santee, M. L., Zurek, R. W., & Waters, J. W.
842 (1997). MLS observations of Arctic ozone loss in 1996–97. *Geophysical Re-*
843 *search Letters*, *24*(22), 2697–2700. doi: 10.1029/97GL52827
- 844 Manney, G. L., & Lawrence, Z. D. (2016). The major stratospheric final warm-
845 ing in 2016: Dispersal of vortex air and termination of Arctic chemical
846 ozone loss. *Atmospheric Chemistry and Physics*, *16*(23), 15371–15396. doi:
847 10.5194/acp-16-15371-2016
- 848 Manney, G. L., Nathaniel J. Livesey, Michelle L. Santee, Zachary D. Lawrence,
849 Alyn Lambert, Luis F. Millan, ... Ryan A. Fuller (submitted 2020). Record
850 low Arctic stratospheric ozone in 2020: MLS polar processing observations
851 compared with 2016 and 2011. *submitted to Geophysical Research Letters*.
- 852 Manney, G. L., Santee, M. L., Rex, M., Livesey, N. J., Pitts, M. C., Veefkind, P.,
853 ... Zinoviev, N. S. (2011). Unprecedented Arctic ozone loss in 2011. *Nature*,
854 *478*(7370), 469–475. doi: 10.1038/nature10556
- 855 Martineau, P., Wright, J. S., Zhu, N., & Fujiwara, M. (2018). Zonal-mean data
856 set of global atmospheric reanalyses on pressure levels. *Earth System Science*
857 *Data*, *10*(4), 1925–1941. doi: 10.5194/essd-10-1925-2018
- 858 Matsuno, T. (1970). Vertical Propagation of Stationary Planetary Waves in the
859 Winter Northern Hemisphere. *Journal of the Atmospheric Sciences*, *27*(6),
860 871–883. doi: 10.1175/1520-0469(1970)027<0871:VPOSPW>2.0.CO;2
- 861 Matthias, V., Dörnbrack, A., & Stober, G. (2016). The extraordinarily strong and
862 cold polar vortex in the early northern winter 2015/2016. *Geophysical Research*
863 *Letters*, *43*(23), 12,287–12,294. doi: 10.1002/2016GL071676
- 864 Matthias, V., & Kretschmer, M. (2020). The Influence of Stratospheric Wave Reflec-
865 tion on North American Cold Spells. *Monthly Weather Review*, *148*(4), 1675–
866 1690. doi: 10.1175/MWR-D-19-0339.1
- 867 Newman, P. A., Gleason, J. F., McPeters, R. D., & Stolarski, R. S. (1997). Anoma-
868 lously low ozone over the Arctic. *Geophysical Research Letters*, *24*(22), 2689–
869 2692. doi: 10.1029/97GL52831
- 870 Newman, P. A., Nash, E. R., & Rosenfield, J. E. (2001). What controls the temper-
871 ature of the Arctic stratosphere during the spring? *Journal of Geophysical Re-*
872 *search: Atmospheres*, *106*(D17), 19999–20010. doi: 10.1029/2000JD000061
- 873 Newman, P. A., & Rosenfield, J. E. (1997). Stratospheric thermal damping times.
874 *Geophysical Research Letters*, *24*(4), 433–436. doi: 10.1029/96GL03720
- 875 Nie, Y., Scaife, A. A., Ren, H.-L., Comer, R. E., Andrews, M. B., Davis, P., & Mar-
876 tin, N. (2019). Stratospheric initial conditions provide seasonal predictability
877 of the North Atlantic and Arctic Oscillations. *Environmental Research Letters*,
878 *14*(3), 034006. doi: 10.1088/1748-9326/ab0385
- 879 Orsolini, Y. J., Nishii, K., & Nakamura, H. (2018). Duration and decay of Arc-
880 tic stratospheric vortex events in the ECMWF seasonal forecast model. *Quar-*
881 *terly Journal of the Royal Meteorological Society*, *144*(717), 2876–2888. doi: 10
882 .1002/qj.3417
- 883 Perlwitz, J., & Harnik, N. (2003). Observational Evidence of a Stratospheric In-
884 fluence on the Troposphere by Planetary Wave Reflection. *Journal of Climate*,
885 *16*(18), 3011–3026. doi: 10.1175/1520-0442(2003)016<3011:OEOASI>2.0.CO;2
- 886 Petzoldt, K. (1999). The role of dynamics in total ozone deviations from their long-
887 term mean over the Northern Hemisphere. *Annales Geophysicae*, *17*(2), 231–

- 888 241. doi: 10.1007/s00585-999-0231-1
- 889 Polvani, L. M., & Kushner, P. J. (2002). Tropospheric response to stratospheric
890 perturbations in a relatively simple general circulation model. *Geophysical Re-*
891 *search Letters*, *29*(7), 18-1-18-4. doi: 10.1029/2001GL014284
- 892 Polvani, L. M., & Waugh, D. W. (2004). Upward Wave Activity Flux as a
893 Precursor to Extreme Stratospheric Events and Subsequent Anomalous
894 Surface Weather Regimes. *Journal of Climate*, *17*(18), 3548–3554. doi:
895 10.1175/1520-0442(2004)017<3548:UWAFAA>2.0.CO;2
- 896 Rao, J., Garfinkel, C. I., & White, I. P. (2020). Predicting the Downward
897 and Surface Influence of the February 2018 and January 2019 Sudden
898 Stratospheric Warming Events in Subseasonal to Seasonal (S2S) Mod-
899 els. *Journal of Geophysical Research: Atmospheres*, e2019JD031919. doi:
900 10.1029/2019JD031919@10.1002/(ISSN)2169-8996.BRIDGE1
- 901 Scaife, A. A., Karpechko, A. Y., Baldwin, M. P., Brookshaw, A., Butler, A. H.,
902 Eade, R., ... Smith, D. (2016). Seasonal winter forecasts and the stratosphere.
903 *Atmospheric Science Letters*, *17*(1), 51–56. doi: 10.1002/asl.598
- 904 Schoeberl, M. R., & Hartmann, D. L. (1991). The Dynamics of the Stratospheric
905 Polar Vortex and Its Relation to Springtime Ozone Depletions. *Science*,
906 *251*(4989), 46–52. doi: 10.1126/science.251.4989.46
- 907 Schoeberl, M. R., Lait, L. R., Newman, P. A., & Rosenfield, J. E. (1992). The
908 structure of the polar vortex. *Journal of Geophysical Research: Atmospheres*,
909 *97*(D8), 7859–7882. doi: 10.1029/91JD02168
- 910 Scott, R. K., Dritschel, D. G., Polvani, L. M., & Waugh, D. W. (2004). Enhance-
911 ment of Rossby Wave Breaking by Steep Potential Vorticity Gradients in the
912 Winter Stratosphere. *Journal of the Atmospheric Sciences*, *61*(8), 904–918.
913 doi: 10.1175/1520-0469(2004)061(0904:EORWBB)2.0.CO;2
- 914 Shaw, T. A., & Perlwitz, J. (2013). The Life Cycle of Northern Hemisphere Down-
915 ward Wave Coupling between the Stratosphere and Troposphere. *Journal of*
916 *Climate*, *26*(5), 1745–1763. doi: 10.1175/JCLI-D-12-00251.1
- 917 Shaw, T. A., & Perlwitz, J. (2014). On the Control of the Residual Circulation and
918 Stratospheric Temperatures in the Arctic by Planetary Wave Coupling. *Jour-*
919 *nal of the Atmospheric Sciences*, *71*(1), 195–206. doi: 10.1175/JAS-D-13-0138
920 .1
- 921 Shaw, T. A., Perlwitz, J., & Harnik, N. (2010). Downward Wave Coupling between
922 the Stratosphere and Troposphere: The Importance of Meridional Wave Guid-
923 ing and Comparison with Zonal-Mean Coupling. *Journal of Climate*, *23*(23),
924 6365–6381. doi: 10.1175/2010JCLI3804.1
- 925 Shindell, D. T., & Schmidt, G. A. (2004). Southern Hemisphere climate response
926 to ozone changes and greenhouse gas increases. *Geophysical Research Letters*,
927 *31*(18). doi: 10.1029/2004GL020724
- 928 Sigmond, M., Scinocca, J. F., Kharin, V. V., & Shepherd, T. G. (2013). Enhanced
929 seasonal forecast skill following stratospheric sudden warmings. *Nature Geo-*
930 *science*, *6*(2), 98–102. doi: 10.1038/ngeo1698
- 931 Sinnhuber, B.-M., Stiller, G., Ruhnke, R., von Clarmann, T., Kellmann, S., & As-
932 chmann, J. (2011). Arctic winter 2010/2011 at the brink of an ozone hole.
933 *Geophysical Research Letters*, *38*(24). doi: 10.1029/2011GL049784
- 934 Smith, K. L., & Kushner, P. J. (2012). Linear interference and the initiation of ex-
935 tratropical stratosphere-troposphere interactions. *Journal of Geophysical Re-*
936 *search: Atmospheres*, *117*(D13). doi: 10.1029/2012JD017587
- 937 Solomon, S. (1999). Stratospheric ozone depletion: A review of concepts and history.
938 *Reviews of Geophysics*, *37*(3), 275–316. doi: 10.1029/1999RG900008
- 939 Stone, K. A., Solomon, S., Kinnison, D. E., Baggett, C. F., & Barnes, E. A. (2019).
940 Prediction of Northern Hemisphere Regional Surface Temperatures Using
941 Stratospheric Ozone Information. *Journal of Geophysical Research: Atmo-*
942 *spheres*, *124*(12), 5922–5933. doi: 10.1029/2018JD029626

- 943 Strahan, S. E., Douglass, A. R., & Newman, P. A. (2013). The contributions of
 944 chemistry and transport to low arctic ozone in March 2011 derived from Aura
 945 MLS observations. *Journal of Geophysical Research: Atmospheres*, *118*(3),
 946 1563–1576. doi: 10.1002/jgrd.50181
- 947 Tegtmeier, S., Rex, M., Wohltmann, I., & Krüger, K. (2008). Relative importance of
 948 dynamical and chemical contributions to Arctic wintertime ozone. *Geophysical*
 949 *Research Letters*, *35*(17). doi: 10.1029/2008GL034250
- 950 Thompson, D. W. J., & Solomon, S. (2002). Interpretation of Recent Southern
 951 Hemisphere Climate Change. *Science*, *296*(5569), 895–899. doi: 10.1126/
 952 science.1069270
- 953 Thompson, D. W. J., Solomon, S., Kushner, P. J., England, M. H., Grise, K. M.,
 954 & Karoly, D. J. (2011). Signatures of the Antarctic ozone hole in Southern
 955 Hemisphere surface climate change. *Nature Geoscience*, *4*(11), 741–749. doi:
 956 10.1038/ngeo1296
- 957 Thompson, D. W. J., & Wallace, J. M. (1998). The Arctic oscillation signature
 958 in the wintertime geopotential height and temperature fields. *Geophysical Re-*
 959 *search Letters*, *25*(9), 1297–1300. doi: 10.1029/98GL00950
- 960 Thompson, D. W. J., & Wallace, J. M. (2000). Annular Modes in the Extratropi-
 961 cal Circulation. Part I: Month-to-Month Variability. *Journal of Climate*, *13*(5),
 962 1000–1016. doi: 10.1175/1520-0442(2000)013<1000:AMITEC>2.0.CO;2
- 963 Tripathi, O. P., Baldwin, M., Charlton-Perez, A., Charron, M., Eckermann, S. D.,
 964 Gerber, E., . . . Son, S.-W. (2015). The predictability of the extratropical
 965 stratosphere on monthly time-scales and its impact on the skill of tropospheric
 966 forecasts. *Quarterly Journal of the Royal Meteorological Society*, *141*(689),
 967 987–1003. doi: 10.1002/qj.2432
- 968 Tripathi, O. P., Charlton-Perez, A., Sigmond, M., & Vitart, F. (2015). Enhanced
 969 long-range forecast skill in boreal winter following stratospheric strong vor-
 970 tex conditions. *Environmental Research Letters*, *10*(10), 104007. doi:
 971 10.1088/1748-9326/10/10/104007
- 972 Wang, T., Tian, W., Zhang, J., Xie, F., Zhang, R., Huang, J., & Hu, D. (2020).
 973 Connections between Spring Arctic Ozone and the Summer Circulation and
 974 Sea Surface Temperatures over the Western North Pacific. *Journal of Climate*,
 975 *33*(7), 2907–2923. doi: 10.1175/JCLI-D-19-0292.1
- 976 Waugh, D. W., Sobel, A. H., & Polvani, L. M. (2017). What Is the Polar Vortex and
 977 How Does It Influence Weather? *Bulletin of the American Meteorological Soci-*
 978 *ety*, *98*(1), 37–44. doi: 10.1175/BAMS-D-15-00212.1
- 979 White, I. P., Garfinkel, C. I., Gerber, E. P., Jucker, M., Aquila, V., & Oman, L. D.
 980 (2019). The Downward Influence of Sudden Stratospheric Warmings: Associ-
 981 ation with Tropospheric Precursors. *Journal of Climate*, *32*(1), 85–108. doi:
 982 10.1175/JCLI-D-18-0053.1
- 983 White, I. P., Lu, H., & Mitchell, N. J. (2016). Seasonal evolution of the QBO-
 984 induced wave forcing and circulation anomalies in the northern winter strato-
 985 sphere. *Journal of Geophysical Research: Atmospheres*, *121*(18), 10,411–
 986 10,431. doi: 10.1002/2015JD024507
- 987 WMO. (2014). *Scientific Assessment of Ozone Depletion: 2014*. Geneva, Switzer-
 988 land: World Meteorological Organization.
- 989 WMO. (2018). *Scientific Assessment of Ozone Depletion: 2018*. Geneva, Switzer-
 990 land: World Meteorological Organization.
- 991 Xie, F., Ma, X., Li, J., Huang, J., Tian, W., Zhang, J., . . . Yang, Y. (2018). An
 992 advanced impact of Arctic stratospheric ozone changes on spring precip-
 993 itation in China. *Climate Dynamics*, *51*(11), 4029–4041. doi: 10.1007/
 994 s00382-018-4402-1
- 995 Xie, F., Zhang, J., Huang, Z., Lu, J., Ding, R., & Sun, C. (2020). An Estimate of
 996 the Relative Contributions of Sea Surface Temperature Variations in Various
 997 Regions to Stratospheric Change. *Journal of Climate*, *33*(12), 4993–5011. doi:

